BABES-BOLYAI UNIVERSITY
FACULTY OF PHYSICS

DOCTORAL SCHOOL OF PHYSICS

MAGNETIC AND MAGNETOCALORIC PROPERTIES OF SELECTED POLYCRYSTALLINE AND NANOCRYSTALLINE MANGANITES

PhD Thesis summary

PhD Student,
Roman Atanasov

Scientific Adviser,
Prof. Dr. Iosif G. Deac

Cluj-Napoca
-2024-

TABLE OF CONTENTS

Chapter 2: Experimental methods, techniques and instruments

Chapter 3: Structural analysis, electrical and magnetic properties, magnetoresistance, magnetocaloric effect in polycrystalline and nano-sized $La_{0.7}Ba_{0.3}MnO_3$ substituted with Eu, Ho.

Abstract

Perovskite structure is the most common ternary transition metal oxide structure. It takes the form ABO_3 where A-site is occupied by a rare-earth or alkaline-earth ion and B-site is a 3-*d* transition metal. Particularly, Mn-based perovskites exhibit high flexibility in doping and substitution options and strong response to external stimuli such as magnetic field, electric field, pressure, temperature, radiation. Because of strong correlations between lattice, spin and charge degrees of freedom, they show spectacular results, like colossal magnetoresistance, giant magnetocaloric effect, anisotropic magnetostriction, magnetocapacitance, high Seebeck coefficient, spin state transitions, etc. Magnetocaloric effect (*MCE*), specifically, has gathered a lot of attention in the last couple of decades, due to its application in cooling devices. Mn-based perovskites possess high values in *MCE* and serve as a cheaper and "green" alternative to traditional cooling materials. In addition, these compounds can be also produced in nanocrystalline and thin film form, further expanding their properties and implementation.

In this thesis, we investigate structural evolution, magnetic, electrical properties with series of substitutions of several manganites, with particular focus on the values of magnetocaloric effect and magnetoresistance. Our main focus is on investigation and achievement of magnetocaloric effect and Colossal magnetoresistance at near room Curie temperatures, and on investigation of properties which can shed light on future work. The systems in question are: $La_{0.7}Ba_{0.3}MnO_3$ substituted with Eu^{3+} (0.05-0.4), Ho^{3+} (0.03-0.15), Ca^{2+} (0.15-0.25); $Pr_{0.65}Sr_{0.35}MnO_3$ substituted with Ca^{2+} (0.02-0.3), Nd^{3+} (0.05-0.35). All the systems were investigated in polycrystalline and nanocrystalline form and the results were compared. Possible origins of some of the properties are proposed and future development is discussed.

key words: manganites, polycrystalline perovskites; colossal magnetoresistance; nanoparticle perovskites; crystallography; magnetic behavior; phase transition; critical behavior; magnetocaloric effect

Summary

At a certain moment, humanity's understanding of environmental problems catches up with their eagerness and blind desire for quick comfort. In the aftermath, a human being contemplates alone in silence and realizes that more efficient and less harmful methods for producing energy are required. These should include: better engines which rely less on fossil fuels, industry which produces less harmful gases and waste that does not pollute our environment.

Some of the proposed solutions or, at least, temporary fixes, are solar, wind power and greatly underrated nuclear power. One of the more environmentally friendly areas of research are the magnetic properties of materials. Among them, transition metal oxides show a wide variety of properties, strong coupling between electrical, thermal and magnetic properties. These compounds have revealed specific properties which are already under more meticulous investigation. Colossal magnetoresistance (CMR) is being researched in order to improve electrical devices and high magnetocaloric effect (MCE) can be implemented for cooling in cryogenics and in many other devices [4-7].

In this work, we will present an investigation of magnetic and electrical properties of Mn^{+}-based perovskite oxides, focusing on Colossal magnetoresistance and Magnetocaloric effect. First chapter is structured as follows: Initially, we will present a brief overview of perovskite structure and its properties. Secondly, we will discuss specific phenomena such as charge ordering, orbital ordering, phase separation, relevant exchange mechanisms, mean field theory and brief overview of other critical behavior models. Next we will present Colossal magnetoresistance and more in depth, Magnetocaloric effect and their methods of measurements.

Chapter 1 will introduce the reader to the theoretical aspects of the research, including the structure of peroskites, variety of electronic, orbital and molecular construction and their possible effect of the physical properties. Brief explanation will be presented into the critical behavior of managnites as well as theoretical considerations of Colossal magnetoresistance and magnetocaloric effect.

Chapter 2 will present the technical methods used to obtain the studied compounds, including solid state reaction and sol-gel method. In addition, we will present methods and instrumentation used for sample structural characterization and investigation of their electrical and magnetic properties.

Chapter 3 will present our results from investigation of $La_{0.7}Ba_{0.3}MnO_3$ substituted with Eu^{3+} (0.05-0.4), Ho^{3+} (0.03-0.15) in polycrystalline and nanocrystalline form with particular focus on their resistivity and magnetocaloric properties.

Chapter 4 will present our results from investigation of $La_{0.7}Ba_{0.3}MnO_3$ substituted with Ca^{2+} (0.15-0.25) in polycrystalline and nanocrystalline form with particular focus on their resistivity and magnetocaloric properties.

Chapter 5 provides result from our investigation into $Pr_{0.65}Sr_{0.35}MnO_3$ substituted with Ca^{2+} (0.02-0.3) in polycrystalline and nanocrystalline form. As with chapter 3 and 4, the focus will be on the electrical and magnetocaloric properties.

Chapter 6 provides result from our investigation into $Pr_{0.65}Sr_{0.35}MnO_3$ substituted with Nd^{3+} (0.05-0.35), in polycrystalline and nanocrystalline form. As with chapter 4, the focus will be on the electrical and magnetocaloric properties.

Chapter 7 will conclude the main points of our research and will propose several avenues for future experimentation based on the results obtained in this work.

1. Introduction

ABX_3 is a perovskite structure where A-site and B-site form cubic structures each and X forms an octahedron with B-site as the center. Most commonly, rare-earth elements take place at A-sites, but similarly sized alkaline-earth can take their place or replace them when doping is needed. The options do not stop there, as even organic molecules can sit at sites, for example, $CH_3NH_3PbI_3$ is used in solar cell research [15]. Smaller 3*d*-transition metals ions occupy B-sites; X-site can host I^- or Cl^- ions, but O^- is by far the most abundant and convenient.

One of the main reasons for scientific interest in Manganite oxides is due to discovery of Colossal Magnetoresistance (*CMR*) effect [5,7]. A competition between Jahn –Teller effect and double exchange, magnetoresistance is defined as percentage change of resistivity under a magnetic field in relation to its absence. Many manganites have shown order of magnitude change in resistivity upon application of an external magnetic field.

The magnetocaloric effect (MCE) is the change in adiabatic temperature (ΔT_{ad}) due to a change in the magnetization of the material. In scientific circles, magnetocaloric effect, more often than not, is defined as the isothermal magnetic entropy change (ΔS_m) as opposed to the change in adiabatic temperature [27]. This intrinsic property is exhibited by all ferromagnetic materials. In MCE process, demagnetized sample is placed in a magnetic field *H*. As a result, randomly oriented spins align with the field. The energy required to "turn" the spins and keep them aligned also affects the lattice, increasing the vibrations. The next step in magnetic refrigeration is to remove the excess heat. This is done via contact with a heat sink which brings the system back to its original temperature *T*. As the external field is removed, electron spins return to their preferred random orientation, increasing spin entropy. Of course, to compensate and find an equilibrium, lattice entropy decreases, thus lowering overall temperature $T - \Delta T$.

The value of MCE is greatly affected by the order of phase transition. A careful combination of first order and second order transitions can increase MCE and help refrigeration [68, 27]. Structure, disorder, doping level, vacancies, type of exchange, all play a crucial role in magnitude of MCE. In addition, it is influenced by the critical behavior of the system. The mean field theory (*MFT*) or

the mean field approximation estimates the behavior quite well, but it is not always applicable. 3D Heisenberg model and Tricritical mean field model describe the systems at different dimensionality and range. Most compounds are well described by one of these models.

Research for high values of magnetocaloric effect are not limited to room temperature range. Paramagnetic salts used in modern state-of-the-art cooling systems (adiabatic demagnetization refrigerators) show large *MCE* at temperatures below 1K. Therefore, investigation of low temperature *MCE* in materials such as manganites can garner attention.

To summarize, here are some of the most important properties of manganites for use in refrigeration and other applications: they are relatively cheap to produce and are chemically stable; they exhibit remarkably wide variety of useful properties, including large thermopower, colossal magnetoresistance, and giant magnetocaloric effect; peak *MCE* happens at T_c which can be tuned by hole doping to be in the temperature range of 10 K – 400 K; structural, ferromagnetic and anti-ferromagnetic phase transitions enhance entropy change ΔS_m and produce normal and inverse *MCE*.

2. Experimental methods, techniques and instruments.

This chapter is focused on the experimental techniques used to produce and characterize Mn-based perovskites. General and particular methods used in these experiments are introduced. Details of sample preparation methods, *VSM*, *XRD*, four-point resistivity measurement cryogenic system, electron microscopy: *TEM*, *SEM*, Iodometry are discussed.

2.1 Sample preparation.

There are several methods for bulk and nano-crystalline sample preparation. In this work, solid-state reaction and sol-gel methods were used due to their simplicity, availability and excellent results [106]. High purity precursors are required for good samples and they were obtained via Alfa Aesar.

2.1.1 Solid-state method

There is reason as to why classics become classics. It is because they work regardless of changing circumstances. As such, solid state reaction fits the bill. It involves mixing precursor powders by hand, pressing them into pellets, calcination and finally, sintering them to their final form. Precisely measured precursors are dehydrated and then placed in a mortar and grinded by a pestle for at least 3 hours. Next, the mixture, still in powder form, is placed in an oven at 1100°C for 24 h for calcination. This achieves the conversion of carbonates into oxides, the removal of unwanted elements such as CO_2 and initiates the reaction. After, the powder is pressed into a pellet of 10 mm width under 3 tons. Lastly, the pellet is sintered at 1350°C for 30 h. The temperature is chosen based on the phase diagrams of the substances. It must be below the melting point but high enough to promote diffusion.

2.1.2 Sol-gel method.

Sol-gel method belongs to the class of wet chemical methods..

In our experiments, Nitrates of metal precursors were chosen. The first state of the process involves dissolving exactly measured nitrates in pure water (18.2 MΩ × cm at 25°C) at 60°C for up to 1h. After, 10 g of sucrose is added to the mix. Such mixing allows positive ions to bond to OH^- hubs of the sucrose chain. After more mixing for 45 minutes, 2 g of pectin is added. This blend is further mixed for 20 minutes. Second step dries the solution in a sand-bath at 100°C for 24 h or until it is visibly dry, which can take up to 3 days. Finally, xero-gel is burned in an oven with high oxygen flow at 1000°C for 2 h.

2.2 Characterization methods

2.2.1 X-ray diffractometer

Amid the plethora of characterization techniques and equipment, X-ray diffraction (XRD) is the "bread and butter" of every solid-state investigation.

Solid bodies can be regarded as a uniform arrangement of evenly spaced ions or atoms. If the interplanar distance is *d* and the incident x-ray has the wavelength on the scale of this distance *d,* then constructive diffraction occurs according to Bragg's law [109, 113].

The diffraction pattern can be analyzed to determine compound composition, purity, cell size and lattice dimensions. We have implemented the use of Williamson-Hall method for determining crystallite size. In addition, we have used Fullprof Rietveld refinement analysis to determine lattice size and structure.

2.2.2 Magnetic measurements (Vibrating magnetometer)

Magnetic measurements were done in a Vibrating Sample Magnetometer (VSM) set-up - CFM-12 T cryogen-free magnet system (Cryogenic Ltd.). Magnetization *M(T, H*) was recorded in varying external fields in the temperature range of 4 – 400 K. The system has the ability to achieve temperature ranges of 1 – 600 K. Superconducting coil is able to produce magnetic flux density up to 12 T. For measurements of field cooled response, a field of 0.05 T was used, while calculation of isothermal magnetization required fields of up to 4 T.

2.2.3 Resistivity measurements. Four point cryogenic resistivity measurement set up

This equipment consists of a cryostat, a measuring rod, four-point chip and a computer conrolling and processing conditions and results [109].
Cryostat is a device used to maintain low temperature of the sample. We used a CFM- 7 T cryogen-free magnet system (Cryogenic Ltd.) working in the temperature range from 5 K to 300 K and

magnetic fields up to 7 T. The gryogen free systen uses pulse tube cryocooler to achieve 4K temperatures and liquification of Helium in the magnet and sample space.
The key to this set up is the four point measuring chip. The advantage of four terminal set up is understood in comparison to the disadvantages of two terminal set up. While sending current through the only two wires and measuring the resistance of the sample, the resulting resistance will include the values of inherent resistance of the wires. For large values of sample resistance, this may be a sufficient measurement method, but for small values, a more sensitive, four point system is a better implement as it gets rid of the wire resistance. The calculation of resistance is done using the well known Omh's law.

2.2.4 Scanning electron microscope (SEM), Transmission electron microscope (TEM) and optical microscope

Imaging of the samples was rendered possible through Scanning and Transmission electron microscopy (SEM and TEM), as well as in an optical microscope. Transmission electron microscopy is another instrument used for characterization of samples. For this study, *TEM* was applied on nanocrystalline compounds.

If one desires only surface knowledge of the sample, optical, or also-called light microscopy can do the job. These sizes were later compared to Rietveld and W-H approximations for all bulk samples.

2.2.5 Iodometry

Magnetic and electric properties of manganite oxides depend on the Mn^{3+}- O - Mn^{4+} relationship. Of course, if some of the oxygen atoms are removed, the overall strength of magnetism can suffer; the ratio Mn^{+3}/Mn^{+4} changes by decreasing the number of Mn^{+4} ions. On the other hand, it is also possible to have an excess of oxygen. This will cause the change in Mn^{+3}/Mn^{+4} ratio by increasing the number of Mn^{+4} ions [118, 119].

Iodometry is a chemical titration process that estimates the amount of Mn^{+3} vs Mn^{+4} by dissolving the sample in acid, then forcing negative acid ions to react with Iodine ions which is, finally, titrated using sodium thiosulfate. The result is then backtracked through balanced chemical equations to calculate the amount of Mn^{+} ions in the first reaction.

Chapter 3. Structural analysis, electrical and magnetic properties, magnetoresistance, magnetocaloric effect in polycrystalline and nano-sized $La_{0.7}Ba_{0.3}MnO_3$ substituted with Eu, Ho.

3.1 Introduction

Perovskites with the formula $RE_{1-x}AE_x(Mn^{3+}/Mn^{4+})O_3$ possess a plethora of interesting properties based on strong spin, charge, orbital and lattice degrees of freedom. Manganites, possessing decent values of entropy change [44, 93, 96, 100], jump ahead of the competition by having the ability to be manipulated for desirable transition temperatures by changing the structure of the lattice. In this work, we have used an opportunity to investigate a series of compounds. As a parent system, for this chapter, we took polycrystalline $La_{0.7}Ba_{0.3}MnO_3$ which exhibits a *PM/FM* transition at T_c = 336 K, (340 K for $La_{0.67}Ba_{0.33}MnO_3$) [102,121,122]. From previous work, it is known that La – based compounds exist in *FMM* state under the transition temperature T_C, while Eu^{3+} – based compounds show *FMI* (ferromagnetic insulator) behavior. On the other hand, Ho^{3+} – based manganites exhibit a more complex phase diagram, mostly *AFM*-ferroelectric, with T_N = 72 K. The parent compound $La_{0.7}Ba_{0.3}MnO_3$ in nano-scale form exhibits a shifted Curie temperature which is attributed to crystalline size, and surface defects where broken bonds and canting of spins lead to lower correlation [127, 128]. Addition of smaller sized ions at the A-site is expected to lower Curie temperature even more.

3.3 Results and discussion

3.3.1 Polycrystalline and nano-scale $La_{(0.7-x)}Eu_xBa_{0.3}MnO_3$ (x = 0, 0.05, 0.1, 0.2, 0.3, 0.4)

3.3.1.1 Structural characterization of polycrystalline $La_{(0.7-x)}Eu_xBa_{0.3}MnO_3$

Polycrystalline systems remain in Rhombohedral, space group *R-3c*, lattice symmetry. Inclusion of Europium changes Mn^{3+} – O – Mn^{4+} angle, increasing the bandwidth. The results of Rietveld refinement show that lattice dimension a(Å) and cell volume V(Å^3) both lower with addition of Eu^{3+}. This is, foremost, caused by the smaller ionic radius of Eu^{3+} ions (1.12 Å) compared to La^{3+} radius (1.216 Å) [130]. Smaller Eu^{3+} ions also introduces disorder and leads to shortening of Mn - O bond lengths. For bulk polycrystalline samples, grain size increases with increase of substitution, varying between 3 - 10 μm.

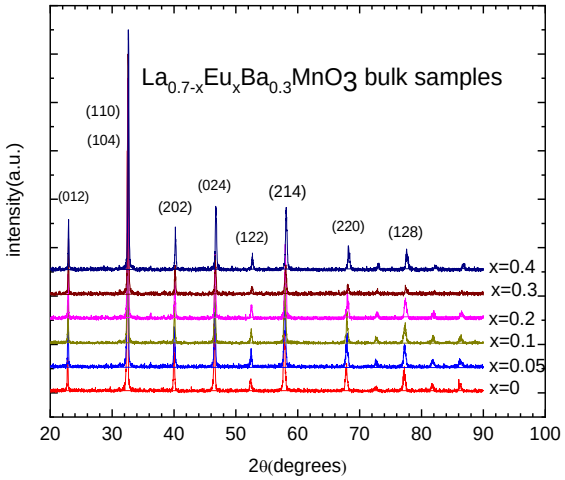

Figure 3.1. X-ray diffraction patterns for $La_{0.7-x}Eu_xBa_{0.3}MnO_3$ polycrystalline samples [131]

Oxygen content investigation via Iodometry showed oxygen deficiency in polycrystalline samples. All bulk $La_{0.7-x}Eu_xBa_{0.3}MnO_3$ compounds exhibited oxygen deficit in the range of 2.97 -2.99 instead of ideal 3. Relative standard deviation of maximum 2.69% makes these measurements reliable.

3.3.1.2 Structural characterization of nano-scale $La_{(0.7-x)}Eu_xBa_{0.3}MnO_3$

In contrast to polycrystalline samples, nano-sized samples exhibit wider pattern peaks. This is due to smaller crystallite sizes which differ from each other in reflective angle for the X-rays. Rietveld refinement analysis confirms the *R3c* space group for all samples just as with bulk compounds. Lattice dimensions also tend to decrease with increasing Eu^{3+} substitution caused by smaller ionic radius of Eu^{3+} compared to La^{3+}, but in contrast, they do not diminish linearly. Overall cell volume gets smaller.

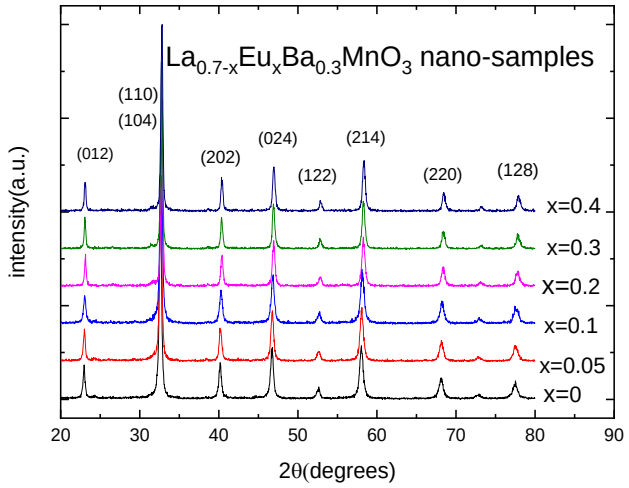

Figure 3.2. X-ray diffraction patterns for $La_{0.7-x}Eu_xBa_{0.3}MnO_3$ nano-sized samples [132]

For nano-samples, *TEM* investigation revealed particle size variation to be between 30 - 70 nm.

All nano-sized particles exhibit slight oxygen excess, with the highest being $O_{3.02}$. This result can be attributed to high surface to volume ratio of the particles, where on the surface, bonds are broken creating more of Mn^{4+} ions [126].

3.3.1.3. Electrical properties of polycrystalline $La_{0.7-x}Eu_xBa_{0.3}MnO_3$

Electrical resistivity measurements on the bulk compounds exhibit behavior common for many ferromagnetic manganites, particularly sharp metallic-insulator transition at T_p. This transition temperature is associated with magnetic *PM* to *FM* transition T_c but is shifted to lower temperature based on strong grain boundary semi-conducting effects. With application of external magnetic fields, T_p is shifted to higher temperatures increasing conductivity. All compounds show classical *CMR* trends. Negative *MR* increases with Eu substitution reaching 63% for x = 0.3.

Sample with x = 0.4 is a special case in this system, showing a semi-conducting exponential jump in resistivity below its T_p temperature. The best fit for this is *VRH* model for a three-dimensional system: $\rho(T) = \rho_0 \exp (T_0/T)^{0.25}$.

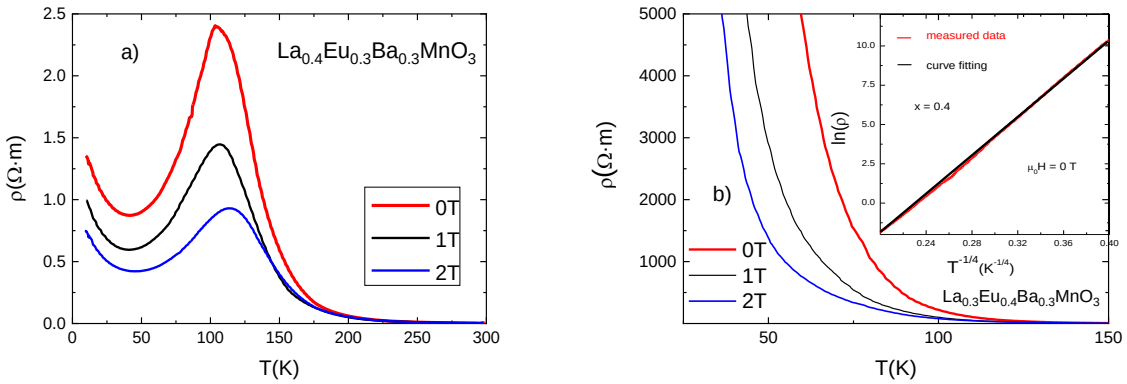

Figure 3.3. Resistivity vs temperature graphs for $La_{0.7-x}Eu_xBa_{0.3}MnO_3$ (a) x = 0.3 and (b) x=0.4. The inset shows the fitting of ln(ρ) as a function of $T^{-1/4}$ for $\mu_0 H$ = 0 T [132].

An interesting feature can be seen in samples with x = 0, 0.05, 0.1, 0.2 and 0.3. At low temperatures, at around 30 - 40 K, an upturn in resistivity is observed. It is explained by an increase in scattering due to intra-grain conditions and external boundary behavior [134]. At low temperatures, electrical conductivity at the grain boundaries depreciates, caused by high disorder.

Table 3.1. Experimental values for $La_{0.7-x}Eu_xBa_{0.3}MnO_3$ bulk materials: electrical properties [132]

Compound (bulk)	T_C(K)	T_P(K)	ρ_{peak} (Ωcm) in 0 T	*MR*max (%) (1T)	*MR*max (%) (2T)
$La_{0.7}Ba_{0.3}MnO_3$	340	295	0.693	5.8	12.9
$La_{0.65}Eu_{0.05}Ba_{0.3}MnO_3$	297	256	0.812	4.2	11.8
$La_{0.6}Eu_{0.1}Ba_{0.3}MnO_3$	270	220	0.084	32.9	52.6
$La_{0.5}Eu_{0.2}Ba_{0.3}MnO_3$	198	165	21.753	22.7	42.1
$La_{0.4}Eu_{0.3}Ba_{0.3}MnO_3$	142	103	240.455	40.4	63.6
$La_{0.3}Eu_{0.4}Ba_{0.3}MnO_3$	99	-	$100 \cdot 10^9$	-	-

3.3.1.4 Magnetic properties of polycrystalline $La_{0.7-x}Eu_xBa_{0.3}MnO_3$ compounds

Measurements of magnetization *FC* and *ZFC* regimes manifest *FM* ordering below T_c and *PM* ordering above T_c. Same typical ferromagnetic behavior is observed in isothermal *M vs* $\mu_0 H$ graphs, where all samples exhibit a steep rise in initial magnetization at temperatures below T_c. The sample with x = 0.05 has the transition from *PM* to *FM* very close to room temperature at 297 K and x = 0.1 sample undergoes transition at 270 K.

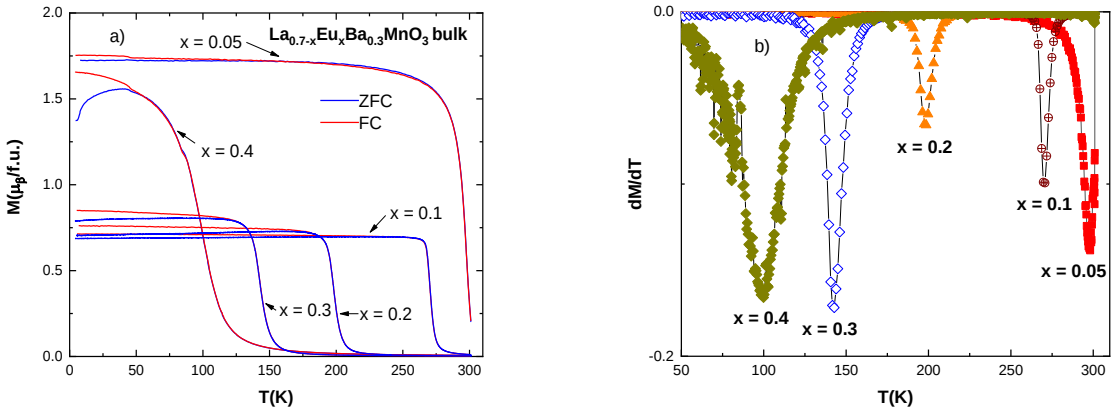

Figure 3.4. a) *ZFC-FC* curves in $\mu_0 H$ = 0.05 T and b) derivative of magnetization for bulk $La_{0.7-x}Eu_xBa_{0.3}MnO_3$ samples [132].

3.3.1.5 Magnetic properties of nano-sized $La_{0.7-x}Eu_xBa_{0.3}MnO_3$ compounds

Corresponding nano-sized compounds experiences lower T_c. Each following increase of Eu content decreases T_c.

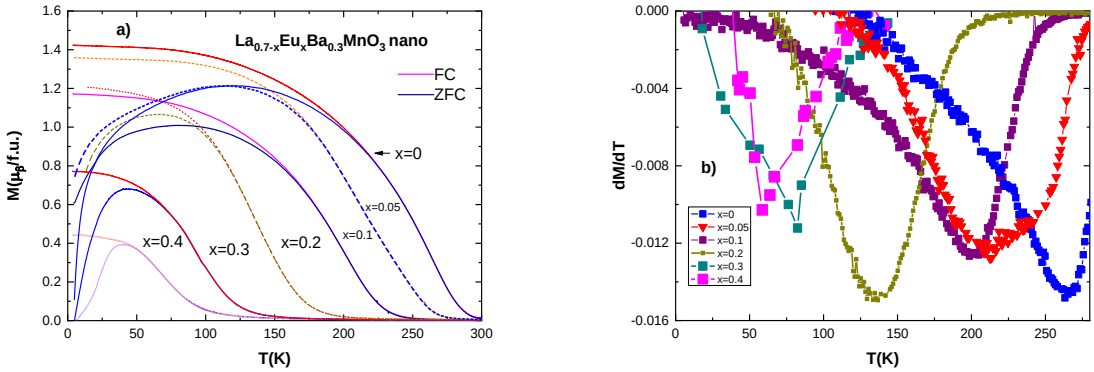

Figure 3.5 *ZFC-FC* curves of magnetization for $La_{0.7-x}Eu_xBa_{0.3}MnO_3$ a) nano-scale samples in $\mu_0 H$ = 0.05 T and b) derivatives *dM/dT* of nano-scale samples [132].

While the sample with x=0.05 for bulk has T_c at 297 K, same x = 0.05 for nano-compound shows T_c = 220 K. Every subsequent sample with larger Eu^{3+} substitution lowers Curie temperature T_c: 200 K for x=0.1, 136 K for x = 0.2, 90 K for x=0.3 and 64 K for x=0.4. Non-linear drop in T_c temperatures of nano-sized particles should be associated with difference in average nano-particle size.

3.3.1.6 Critical magnetic behavior of polycrystalline $La_{0.7-x}Eu_xBa_{0.3}MnO_3$ samples

Arrott plots confirm second-order phase transition for all compounds. Construction of Modified Arrot plots revealed an interesting difference between the two systems: all bulk compounds are governed by tri-critical mean field model and all nano-sized compounds are governed by conventional mean field model.

Table 3.2. Critical exponents values for polycrystalline and nano-scale $La_{0.7-x}Eu_xBa_{0.3}MnO_3$ samples [132].

compound		γ	β	δ	T_c (K)
x=0	bulk	1.065	0.288	4.69	340
x=0.05	bulk	0.985	0.234	5.2	297
x=0.1	bulk	1.07	0.245	5.37	270
x=0.2	bulk	0.976	0.276	4.54	198
x=0.3	bulk	0.983	0.255	4.85	142
x=0.4	bulk	1.022	0.249	5.10	99
x=0	nano	1.164	0.493	3.36	263
x=0.05	nano	1.27	0.538	3.36	220
x=0.1	nano	1.112	0.521	3.13	200
x=0.2	nano	1.111	0.461	3.41	136
x=0.3	nano	1.224	0.537	3.28	90
x=0.4	nano	1.198	0.512	3.34	64
Mean field model		1	0.5	3	
3D-Heisenberg model		1.366	0.355	4.8	
Ising model		1.24	0.325	4.82	
Tricritical mean field model		1	0.25	5	

3.3.1.8 Magnetic entropy change in polycrystalline $La_{0.7-x}Eu_xBa_{0.3}MnO_3$ compounds

$La_{0.7-x}Eu_xBa_{0.3}MnO_3$ samples are ferromagnetic throughout and undergo second order transition at *PM* to *FM* phase change, the effect of magnetic field on the sample will be to decrease its entropy. Negative magnetic entropy change for all $La_{0.7-x}Eu_xBa_{0.3}MnO_3$ (x = 0, 0.05, 0.1, 0.2, 0.3, 0.4) polycrystalline samples was established. In Figure 3.6, we present selected graphs of $-\Delta S_M$ *vs T* for samples closest to sought after room temperature T_c. Table 3.3 in the next section compares the cooling potential of nano and bulk compounds and shows the values of entropy change for all of the samples.

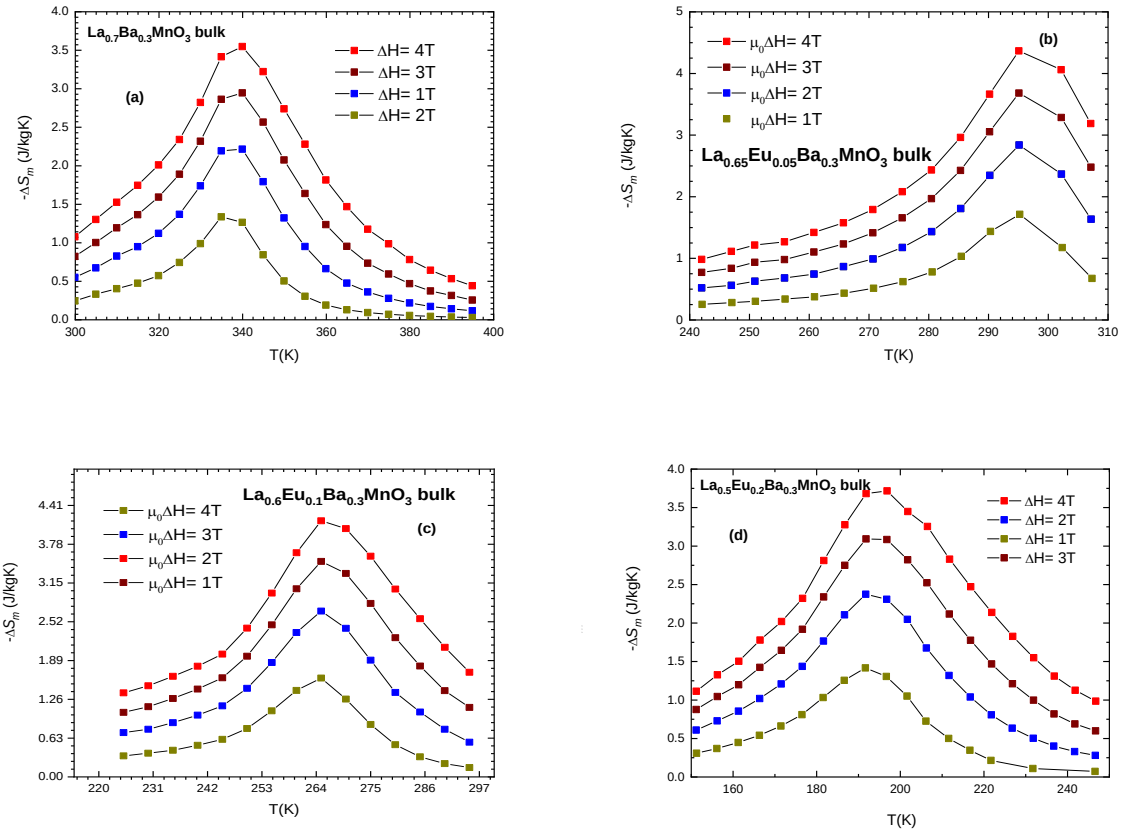

Figure 3.6 Magnetic entropy change vs temperature (-ΔS_M vs T) graphs for several bulk $La_{0.7-x}Eu_xBa_{0.3}MnO_3$ samples with the closest to room temperature T_c. a) x=0 b) x=0.05 c) x=0.1 d) x=0.2 [132]

Maximum entropy change is exhibited by the sample with Eu content of x = 0.05 $|\Delta S_M|$ = 4.2 J/kgK at 4 T and for x = 0.1 with $|\Delta S_M|$ = 4.1 J/kgK at the same field while the parent compound possesses $|\Delta S_M|$ = 3.5 J/kgK.

3.3.1.9 Magnetic entropy change in nano-scale $La_{0.7-x}Eu_xBa_{0.3}MnO_3$ compounds

Nano-sized particles show lower entropy change values. As a positive, they exhibit a much wider temperature range δT_{FWHM} with some exceeding 90 K. For example, while bulk x = 0.05 at 4 T shows $|\Delta S_M|$ = 4.2 J/kgK, same nano-sample has $|\Delta S_M|$ = 1.63 J/kgK. All samples exhibit values under 2 J/kgK. All the values can be seen in the Table 3.3 in the next section.

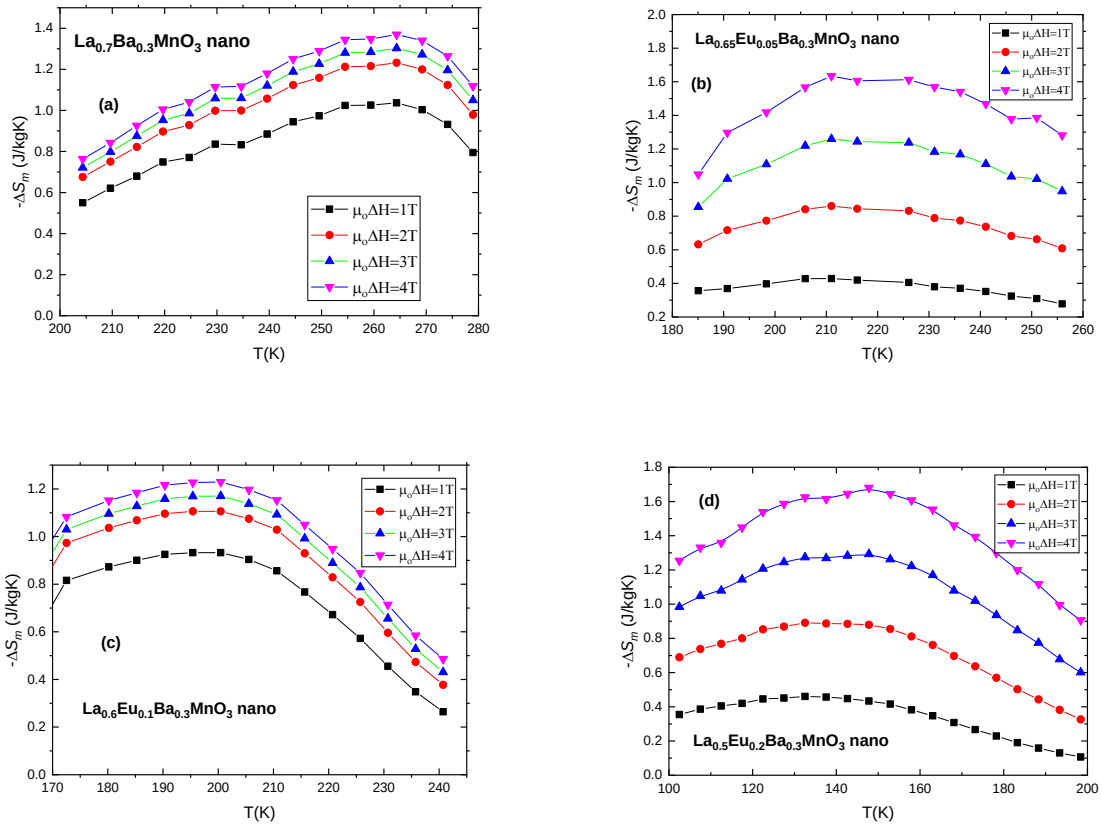

Figure 3.7 Magnetic entropy change vs temperature ($-\Delta S_M$ vs T) graphs for several nano $La_{0.7-x}Eu_xBa_{0.3}MnO_3$ samples with the closest to room temperature T_c. a) x=0 b) x=0.05 c) x=0.1 d) x=0 [132].

3.3.1.10 Magnetocaloric effect in polycrystalline and nano-scale

$La_{0.7-x}Eu_xBa_{0.3}MnO_3$

Table 3.3 lists *RCP* values for all compounds, including bulk and nano-scale samples. We can see that, for bulk, the initial introduction of Eu^{3+} ions into the system does not increase *RCP* for any values of applied magnetic field, although its maximum entropy change increases from the parent compound. Temperature range at half maximum is smaller, or in other words, the curve of the peak is narrower than for the parent sample.

Application of stronger fields leads to increase in peak entropy change and in the width of the peaks, hence, increase in *RCP*. At $\mu_0\Delta H = 4$ T values augment to values which are quite large, comparable with the best values of other researched manganites [4, 153, 154, 155, 156, 157].

Table 3.3. Experimental values for $La_{0.7-x}Eu_xBa_{0.3}MnO_3$ materials: magnetic and magnetocaloric measurements [132].

Compound	T_C (K)	M_s (μ_B/f.u.)	M_r (μ_B/f.u.)	M_r/M_sH_{ci}(Oe)		$\lvert\Delta S_M\rvert$ (J/kgK) $\mu_0\Delta H$ = 1 T	$\lvert\Delta S_M\rvert$ (J/kgK) $\mu_0\Delta H$ = 4 T	$RCP(S)$ (J/kg) $\mu_0\Delta H$ = 1 T	$RCP(S)$ (J/kg) $\mu_0\Delta H$ = 4 T	*Refs*
$La_{0.7}Ba_{0.3}MnO_3$ (bulk)	340	4.04	0.24	0.06	200	1.33	3.5	53.7	158.4	This work
$La_{0.65}Eu_{0.05}Ba_{0.3}MnO_3$	297	3.87	0.57	0.15	172	1.71	4.2	42.7	155.4	This work
$La_{0.6}Eu_{0.1}Ba_{0.3}MnO_3$	270	3.84	0.64	0.17	63	1.6	4.1	40	187.7	This work
$La_{0.5}Eu_{0.2}Ba_{0.3}MnO_3$	198	3.7	0.22	0.06	67	1.41	3.7	38.1	212.6	This work
$La_{0.4}Eu_{0.3}Ba_{0.3}MnO_3$	142	3.78	0.4	0.11	66	1.7	3.5	42.6	176.4	This work
$La_{0.3}Eu_{0.4}Ba_{0.3}MnO_3$	99	3.46	0.54	0.16	120	1.02	2.83	25.7	133.3	This work
$La_{0.7}Ca_{0.3}MnO_3$	256					1.38		41		44
$La_{0.7}Sr_{0.3}MnO_3$	365					-	4.44(5T)		128(5T)	44
$La_{0.6}Nd_{0.1}Ca_{0.3}MnO_3$	233					1.95		37		44
$Gd_5Si_2Ge_2$	276					-	18(5T)	-	535(5T)	44
Gd	293					2.8		35		44
$La_{0.7}Ba_{0.3}MnO_3$(nano)	263	2.79	1.16	0.41	480	1.04	1.37	105.4	130.1	This work
$La_{0.65}Eu_{0.05}Ba_{0.3}MnO_3$(nano)	220	2.95	0.84	0.28	410	0.43	1.63	43.3	155.6	This work
$La_{0.6}Eu_{0.1}Ba_{0.3}MnO_3$(nano)	200	2.6	0.88	0.34	390	0.93	1.23	93.5	135.3	This work
$La_{0.5}Eu_{0.2}Ba_{0.3}MnO_3$(nano)	136	2.96	0.78	0.26	280	0.46	1.68	47.8	218.4	This work
$La_{0.4}Eu_{0.3}Ba_{0.3}MnO_3$(nano)	90	2.3	0.83	0.36	590	0.39	1.99	38.3	187.7	This work
$La_{0.3}Eu_{0.4}Ba_{0.3}MnO_3$(nano)	64	2.09	0.63	0.3	960	0.25	1.09	23.3	119.9	This work
$La_{0.67}Ca_{0.33}MnO_3$(nano)	260						0.97(5T)		27(5T)	[154]
$La_{0.6}Sr_{0.4}MnO_3$(nano)	365					1.5		66		[153]
$Pr_{0.65}(Ca_{0.6}Sr_{0.4})_{0.35}MnO_3$(nano)	220					0.75		21.8		[156]

We have estimated *TEC* for all the samples and found that it tends to diminish with expanding temperature range for all compounds; more so prominently for bulk samples because their entropy curve is much smoother and narrower. This means that the most viable use for materials in cooling devices is at shorter temperature ranges ($\Delta T = 5 – 10$ K). In addition, polycrystalline compounds possess higher values of *TEC* compared to their nano-sized counterparts, with the external

magnetic field needing to be $\mu_0\Delta H$ = 4 T in order to match the results from bulk at $\mu_0\Delta H$ = 1 T at around 1.6 J/kgK.

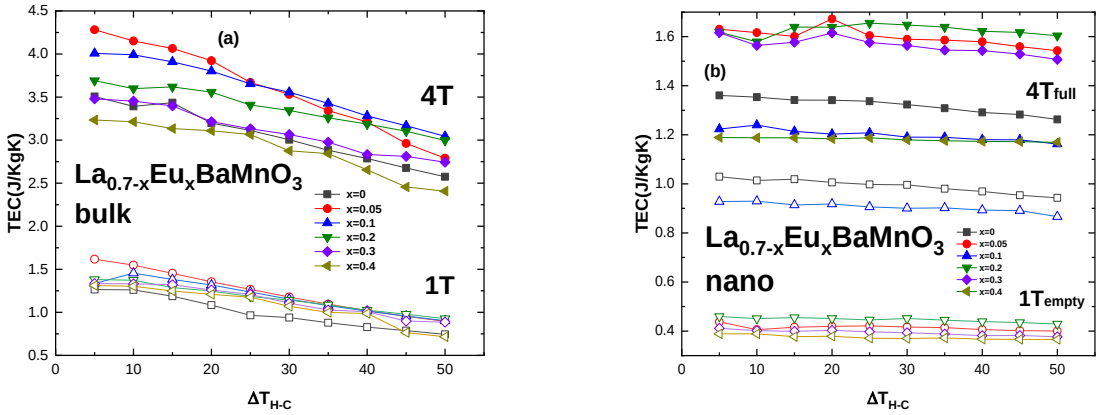

Figure 3.8 Temperature-averaged entropy change (TEC) vs $\Delta T_{H\text{-}C}$ for a) polycrystalline $La_{0.7-x}Eu_xBa_{0.3}MnO_3$ b) nano-sized $La_{0.7-x}Eu_xBa_{0.3}MnO_3$

3.3.2 Polycrystalline and nano-scale $La_{(0.7-x)}Ho_xBa_{0.3}MnO_3$ (x = 0.03, 0.05, 0.1, 0.15)

3.3.2.1 Structural characterization of polycrystalline $La_{(0.7-x)}Ho_xBa_{0.3}MnO_3$

The symmetry of the samples does not change from the parent compound which belongs to Rhombohedral *R3c* space group. Average ionic radius becomes smaller caused by smaller Ho^{3+} ionic radius (1.072 Å) compared to La^{3+} ionic radius (1.216 Å) [130]. This, in turn, causes smaller lattice dimensions and cell volume.

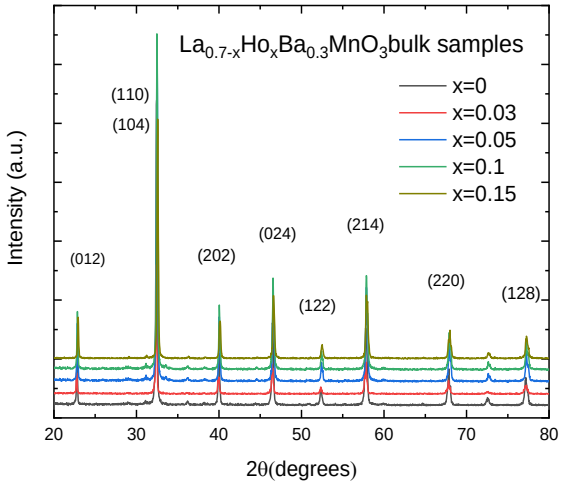

Figure 3.9 X-ray diffraction patters for polycrystalline $La_{0.7-x}Ho_xBa_{0.3}MnO_3$

Preparation of the samples incurred an obstacle in that Ho^{3+} ions prefer to arrange into a hexagonal structure, like $HoMnO_3$ compounds. Here, phase separation was observed in x-ray patterns for samples with high Ho^{3+} content and the bulk compound with x = 0.15 was prepared by quenching the sample in water right after sintering in order to prevent phase separation during the cooling period.

Oxygen stoichiometry was investigated by implementing the iodometric titration method [118]. It reveals oxygen deficiency for all bulk $La_{0.7-x}Ho_xBa_{0.3}MnO_3$ samples.

3.3.2.2 Structural characterization of nano-scale $La_{(0.7-x)}Ho_xBa_{0.3}MnO_3$

Patterns shown in Figure 3.10 reveal a single phase for all compounds with acceptable impurity levels. Further investigation of the patterns by Rietveld refinement method shows that samples possess rhombohedral *R3c* symmetry. In addition, cell volume diminishes compared to the parent nano-compound $La_{0.7}Ba_{0.3}MnO_3$ with each addition of Ho^{3+} ions. On the other hand, lattice dimensions do not diminish linearly, similar to the case with $La_{0.7-x}Eu_xBa_{0.3}MnO_3$ nano-sized particles. Results for cell volume and lattice parameters show that they are smaller than equivalent bulk samples.

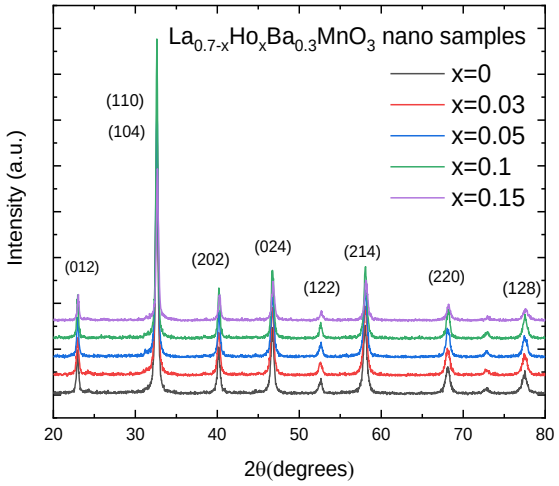

Figure 3.10 X-ray diffraction patterns for nano-scale $La_{0.7-x}Ho_xBa_{0.3}MnO_3$

According to Rietveld refinement analysis, the average particle size of the nano-scale compounds lies in the range of 20 nm except the x = 0.1 sample where Rietveld produced a 82.25 nm estimation. *TEM* shows that average particle for nano-compounds is in the range of 50 - 80 nm. Results from Iodometric titration analysis show that all of the nano-compounds have oxygen excess. The average oxygen formula looks like $O_{3.02\pm0.02}$, meaning that Iodometry revealed a slight excess of Mn^{4+} ions in the compounds.

3.3.2.3. Electrical properties of polycrystalline $La_{0.7-x}Ho_xBa_{0.3}MnO_3$

Investigation of the electrical properties of the polycrystalline compounds, revealed typical *CMR* behavior. All samples experience peak in resistivity T_p associated with metal-insulator transition and it is related to the *FM/PM* magnetic transition at T_c but is shifted to lower temperatures caused by strong grain boundary effect which act as semi-conductors.

All compounds show minimum at the lowest temperatures, at 10 K, in contrast to $La_{0.7-x}Eu_xBa_{0.3}MnO_3$ compounds, which manifest an upturn at low temperatures after a minimum in resistivity.

Maximum resistivity ρ_{peak} (Ωcm) is lowered as the Ho^{3+} content grows after an initial increase. A possible reason for this decrease can be the decrease in the Mn - O bond length and increase in the $Mn^{3+} - O - Mn^{4+}$ angle leading to an increase in metallicity. This behavior was observed in other systems under our investigation, with low substitution levels.

Negative magnetoresistance *MR* has been observed for all bulk samples. It increases from the *MR* values of the parent sample for both 1 T and 2 T field differences.

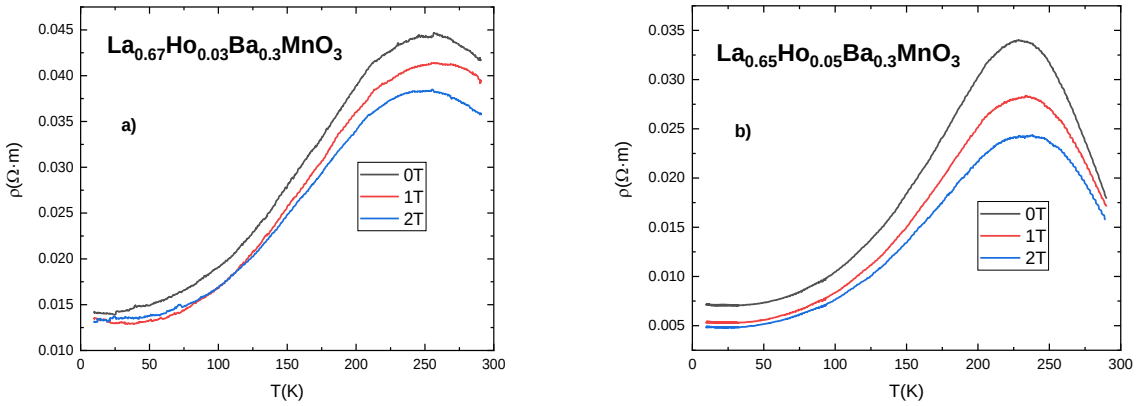

Figure 3.11. Resistivity vs temperature graphs for the bulk $La_{0.7-x}Ho_xBa_{0.3}MnO_3$ samples with (a) x = 0.03 and (b) x=0.05.

Table 3.4. Experimental values for $La_{0.7-x}Ho_xBa_{0.3}MnO_3$ bulk materials: electrical properties.

Compound (bulk)	T_C(K)	T_P(K)	ρ_{peak} (Ωcm) in 0 T	*MR*max (%) (1T)	*MR*max (%) (2T)
$La_{0.7}Ba_{0.3}MnO_3$	340	295	0.693	5.8	12.9
$La_{0.67}Ho_{0.03}Ba_{0.3}MnO_3$	298	256	4.46	7.4	14.4
$La_{0.65}Ho_{0.05}Ba_{0.3}MnO_3$	272	228	3.40	17.2	28.8
$La_{0.6}Ho_{0.1}Ba_{0.3}MnO_3$	223	209	2.82	22.1	36.4
$La_{0.55}Ho_{0.15}Ba_{0.3}MnO_3$	185	165	2.77	27.4	38.7

3.3.2.3 Magnetic properties of polycrystalline $La_{0.7-x}Ho_xBa_{0.3}MnO_3$ compounds

Magnetic measurements in low field cooling and in zero field cooling (ZFC-FC) regimes in the temperature range 4 K - 300 K show typical ferromagnetic behavior. The compounds undergo *PM/FM* phase transition at temperatures T_c. Polycrystalline compounds of x = 0.03 and x = 0.05 reveal near room temperature T_c values. All samples exhibit soft-magnetic behavior.

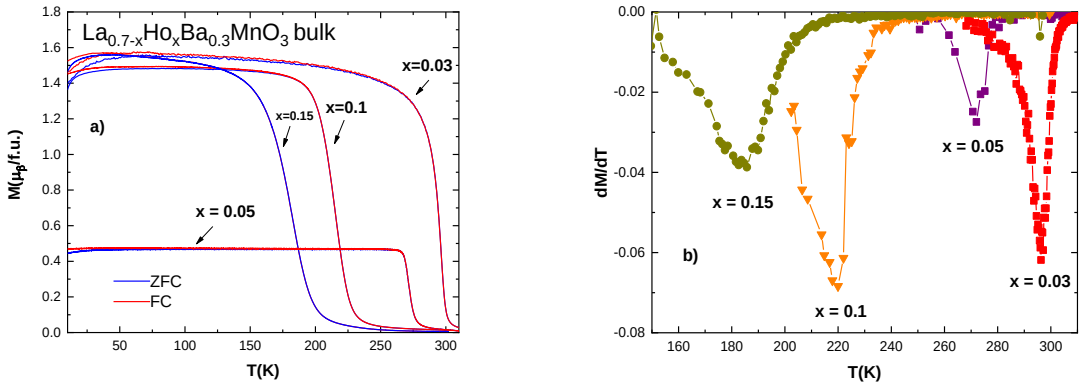

Figure 3.12 a) *ZFC-FC* curves and b) derivative of magnetization for bulk $La_{0.7-x}Ho_xBa_{0.3}MnO_3$ samples.

3.3.2.5 Magnetic properties of nano-scale $La_{0.7-x}Ho_xBa_{0.3}MnO_3$ compounds

Magnetization of the nano-scale samples was investigated *FC* and *ZFC* measurements in the temperature range 4 - 310 K in a field of 0.05 T. Analogous to the bulk samples, every nano-compound exhibits typical magnetic *FM* and *PM* phases. At low temperatures, below blocking temperature, the difference between *ZFC* and *FC* lines is greater than in bulk samples suggesting higher anisotropy. Phase transition occurs more gradually in nano-scale compounds evidenced by a lower slope of the *ZFC-FC* plots at the transition temperature.

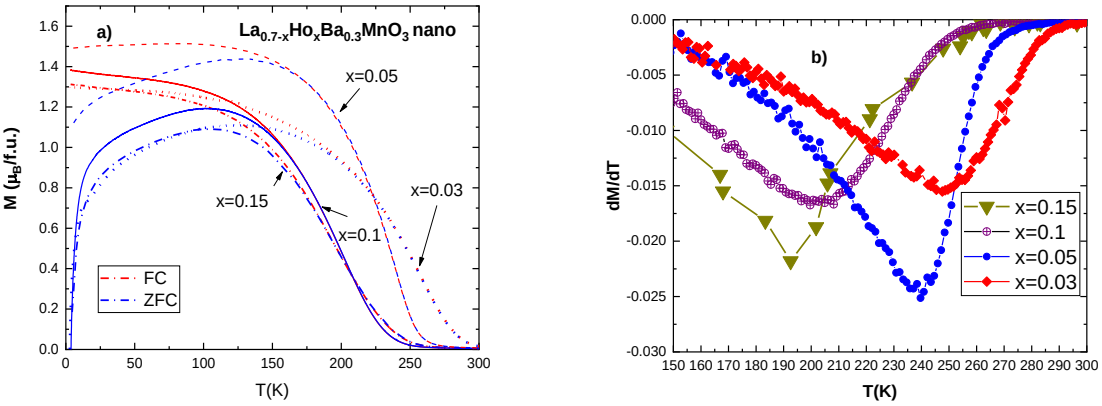

Figure 3.13 a) *ZFC-FC* curves and b) derivative of magnetization for nano $La_{0.7-x}Ho_xBa_{0.3}MnO_3$ samples.

It can be seen in Figure 3.13b, that the derivative does not take a sharp minimum value, confirming a more gradual phase transition.

Curie temperature values are lower than those for the equivalent polycrystalline sample. For instance, sample x = 0.03 exhibits T_c = 251 K, whereas the bulk x = 0.03 sample shows T_c = 298 K.

3.3.2.6 Critical magnetic behavior of polycrystalline $La_{0.7-x}Ho_xBa_{0.3}MnO_3$ samples

Construction of conventional Arrott plots revealed second-order phase transition for all samples. All polycrystalline compounds are governed by the tricritical mean field model for γ exponent related to inverse of susceptibility and by 3D Heisenberg model for β exponent related to spontaneous magnetization. For nano-scale compounds, *MAP* lines look similar to the original Arrott plot lines and are all governed by mean field model.

Table 3.5. Critical exponents values for $La_{0.7-x}Ho_xBa_{0.3}MnO_3$ polycrystalline and nano-scale samples.

compound		γ	β	δ	T_c (K)
x=0	bulk	1.065	0.288	4.69	340
x=0.03	bulk	0.973	0.347	3.8	298
x=0.05	bulk	0.958	0.357	3.68	272
x=0.1	bulk	0.878	0.398	3.21	220
x=0.15	bulk	0.892	0.393	3.28	185
x=0	nano	1.164	0.493	3.36	263
x=0.03	nano	1.073	0.549	2.95	251
x=0.05	nano	0.974	0.515	2.89	239
x=0.1	nano	0.988	0.476	3.08	205
x=0.15	nano	1.072	0.556	2.93	190
Mean field model		1	0.5	3	
3D-Heisenberg model		1.366	0.355	4.8	
Ising model		1.24	0.325	4.82	
Tricritical mean field model		1	0.25	5	

3.3.2.8 Magnetic entropy change in polycrystalline $La_{0.7-x}Ho_xBa_{0.3}MnO_3$ compounds

Isothermal magnetic measurements at temperatures below and above T_c with interval of 5 K were used to calculate entropy change for all samples. In $La_{0.7-x}Ho_xBa_{0.3}MnO_3$ values for maximum entropy change are comparable to other manganite compounds exhibiting only second-order transition. The sample with x = 0.03 exhibits the highest value of entropy change $|\Delta S_M|$, at around T_c, of 5.36 J/KgK in $\mu_o \Delta H$ = 4 T. Possibly another important value to be mentioned is the entropy

change $|\Delta S_M|$ for x = 0.05 sample at $\mu_o \Delta H$ = 1 T, it is highest among all samples at 2.11 J/KgK. This sample possesses near room temperature T_c = 272 K.

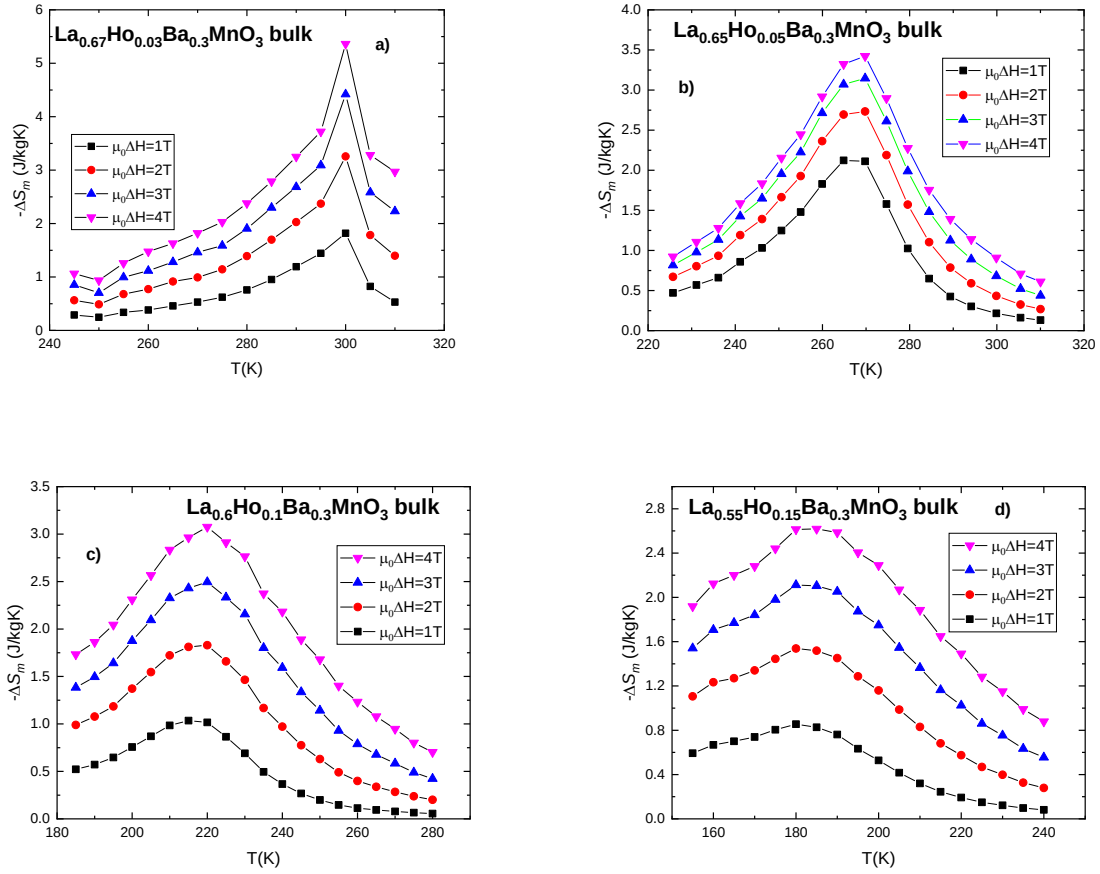

Figure 3.14 Magnetic entropy change vs temperature (-ΔS_M vs T) graphs for bulk $La_{0.7-x}Ho_xBa_{0.3}MnO_3$ samples. a) x=0.03 b) x=0.05 c) x=0.1 d) x=0.15

3.3.2.9 Magnetic entropy change in nano-scale $La_{0.7-x}Ho_xBa_{0.3}MnO_3$ compounds

For nano-scale compounds, the measured entropy change is lower than for their polycrystalline counterparts, but exhibit entropy change values higher than the parent sample except the x = 0.15 compound. The standout sample here is the x = 0.05, which reveals $|\Delta S_M|$ = 1.67 J/KgK in $\mu_o \Delta H$ = 1 T and $|\Delta S_M|$ = 2.15 J/KgK in $\mu_o \Delta H$ = 4 T. The compound x = 0.15 exhibits the lowest entropy change, even lower than the parent compound at 0.4 J/KgK for $\mu_o \Delta H$ = 1 T but it increases its entropy change values with a bigger magnetic field change.

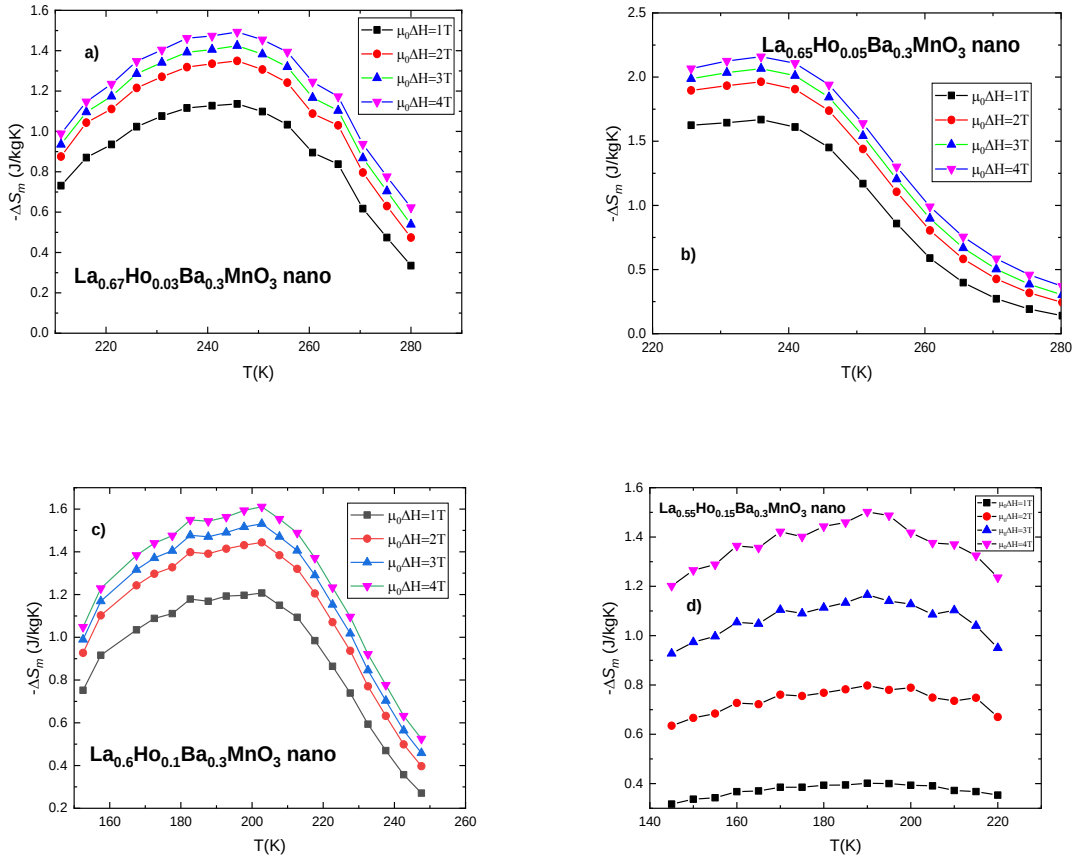

Figure 3.15 Magnetic entropy change vs temperature (-ΔS_M vs T) graphs for nano $La_{0.7-x}Ho_xBa_{0.3}MnO_3$ samples. a) x=0.03 b) x=0.05 c) x=0.1 d) x=0.15

3.3.2.10 Magnetocaloric effect in polycrystalline and nano-scale $La_{0.7-x}Ho_xBa_{0.3}MnO_3$

For nano-sized $La_{0.7-x}Ho_xBa_{0.3}MnO_3$ compounds, width of the entropy change curve is much larger than for the bulk compounds, bringing the values of *RCP* closer together. Bulk samples exhibit larger cooling power at higher fields. Firstly, for $\mu_0\Delta H$ = 1T polycrystalline compounds show an initial drop in *RCP* relative to the parent compound $La_{0.7}Ba_{0.3}MnO_3$. We see that $La_{0.67}Ho_{0.03}Ba_{0.3}MnO_3$ exhibits *RCP* = 36.2 J/Kg, down from 53.7 J/Kg for the parent sample. Nano-sized samples, at $\mu_0\Delta H$ = 1 T, report somewhat larger values of *RCP*, due to their very large values of δT_{FWHM} which can reach 80 – 90 K. At the external magnetic field change of 4 T, things are slightly shifted for the bulk material. Samples x = 0.03 and x = 0.05 having the highest $|\Delta S_M|$ do not show the highest *RCP* at 134 J/Kg and 136 J/Kg respectively.

Table 3.6. Experimental values for $La_{0.7-x}Ho_xBa_{0.3}MnO_3$ materials: magnetic measurements.

Compound	T_C(K)	M_s(μ_B/f.u.)	M_r(μ_B/f.u.)	M_r/M_s	H_{ci}(Oe)	$\lvert\Delta S_M\rvert$ (J/kgK) $\mu_0\Delta H$ = 1 T	$\lvert\Delta S_M\rvert$ (J/kgK) $\mu_0\Delta H$ = 4 T	*RCP*(*S*) (J/kg) $\mu_0\Delta H$ = 1 T	*RCP*(*S*) (J/kg) $\mu_0\Delta H$ = 4 T
$La_{0.7}Ba_{0.3}MnO_3$ (bulk)	340	4.04	0.24	0.06	200	1.33	3.5	53.7	158.4
$La_{0.67}Ho_{0.03}Ba_{0.3}MnO_3$(bulk)	298	3.91	0.62	0.16	80	1.81	5.36	36.2	134
$La_{0.65}Ho_{0.0.05}Ba_{0.3}MnO_3$(bulk)	272	3.98	0.12	0.03	100	2.11	3.42	69.6	136.8
$La_{0.6}Ho_{0.1}Ba_{0.3}MnO_3$(bulk)	220	4.00	0.38	0.09	150	1.04	3.07	52	214.9
$La_{0.55}Ho_{0.15}Ba_{0.3}MnO_3$(bulk)	185	4.07	0.39	0.09	130	0.85	2.62	51.8	209.6
$La_{0.7}Ba_{0.3}MnO_3$(nano)	263	2.79	1.16	0.41	480	1.04	1.37	105.4	130.1
$La_{0.67}Ho_{0.03}Ba_{0.3}MnO_3$(nano)	251	2.94	1.05	0.36	420	1.13	1.49	79.1	104.5
$La_{0.65}Ho_{0.0.05}Ba_{0.3}MnO_3$(nano)	239	3.59	0.89	0.25	310	1.67	2.15	116.9	150.5
$La_{0.6}Ho_{0.1}Ba_{0.3}MnO_3$(nano)	205	3.63	0.97	0.27	380	1.21	1.61	96.8	128.8
$La_{0.55}Ho_{0.15}Ba_{0.3}MnO_3$(nano)	190	3.56	1.01	0.28	450	0.4	1.5	36	135

In addition to *RCP* we have estimated another figure of merit of cooling material – temperature averaged entropy change *TEC*. Calculations were done in temperature intervals of $\Delta T_{H\text{-}C}$ = 5 – 50 K. Polycrystalline samples exhibit high values (Figure 3.16). For nano-compounds, the lines do not slope as much as the bulk sample's lines - the values at $\Delta T_{H\text{-}C}$ = 50 K are not drastically lower than for $\Delta T_{H\text{-}C}$ = 5 K.

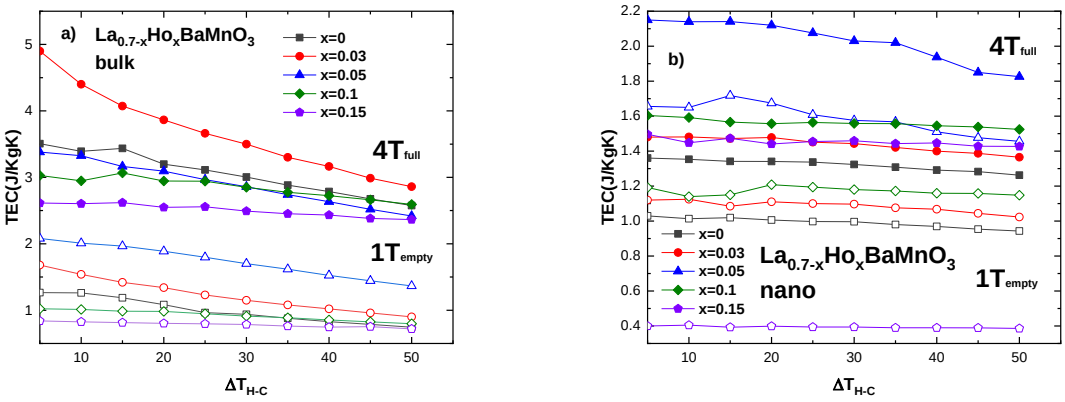

Figure 3.16 Temperature-averaged entropy change (TEC) vs. $\Delta T_{H\text{-}C}$ for a) polycrystalline $La_{0.7-x}Ho_xBa_{0.3}MnO_3$ b) nano-sized $La_{0.7-x}Ho_xBa_{0.3}MnO_3$

Chapter 4. Structural analysis, electrical and magnetic properties, magnetoresistance, magnetocaloric effect in polycrystalline and nano-sized $La_{0.7}Ba_{0.3}MnO_3$ substituted with Ca.

4.1 Introduction

In this chapter we will continue our investigation on the results of substitution on the A-site of the parent compound from chapter 3, namely $La_{0.7}Ba_{0.3}MnO_3$. This time, the substitution with Ca^{2+} ions is intended to replace Ba^{2+} ions in the structure. Ca ions are smaller than Ba ions, thus our purpose is to introduce further mismatch at the A-site. The result should be change in distances between magnetic ions (mainly Mn^{+} ions) and increase of local disorder which can lead to change in electrical and magnetic properties.

4.2 Resuslts and discussion

4.2.1 Structural characterization of polycrystalline $La_{0.7}Ba_{0.3-x}Ca_xMnO_3$ (x = 0.15, 0.2, 0.25)

The inclusion of Ca^{2+} ions into the structure at the A-site decreases the average ionic radius of the site $<r_a>$. This results in stress on the MnO_6 octahedron, causing its distortion. At a certain point of Ca^{2+} inclusion, the structure changes from rhombohedral *R3c* space group to orthorhombic *Pbnm* space group. For our study, this change occurred for Ca^{2+} level x = 0.25. For polycrystalline samples, optical microscopy reveals grain sizes in the range of 1 – 3 μm.

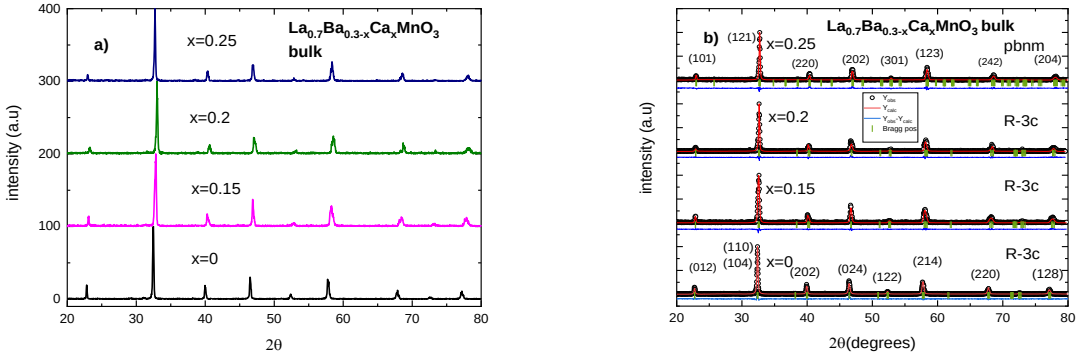

Figure 4.1 a) X-ray diffraction pattern for bulk $La_{0.7}Ba_{0.3-x}Ca_xMnO_3$ and b) results from Rietveld refinement fit showing change of the space group [171].

Finishing structural analysis is the stoichiometric investigation of oxygen content. This was done by carrying out Iodometric titration analysis [118]. It is aimed at estimating the Mn^{3+}/Mn^{4+} ratio and in Table 4.3 we present the results. As with other polycrystalline compounds in this work, oxygen stoichiometry shows a deficit.

4.2.2 Structural characterization of nano-scale $La_{0.7}Ba_{0.3-x}Ca_xMnO_3$ (x = 0.15, 0.2, 0.25)

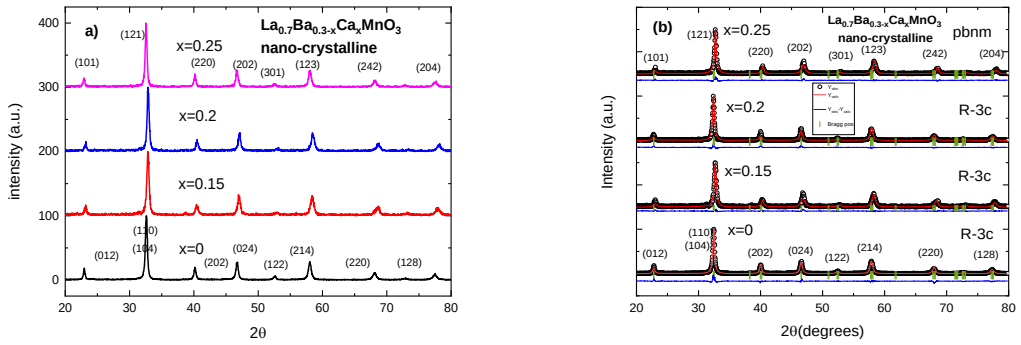

Figure 4.2 a) x-ray diffraction patterns for nano-scale $La_{0.7}Ba_{0.3-x}Ca_xMnO_3$ and b) results from Rietveld refinement fit, with space group change [172].

X – ray diffraction patterns for nano-sized $La_{0.7}Ba_{0.3-x}Ca_xMnO_3$, as seen in Figure 4.2a, reveal peaks which are wider than ones for the polycrystalline compounds, as it is expected due to smaller crystallite size. In Figure 4.3b, the fit from Rietveld refinement shows that the sample x = 0.25, just as with the polycrystalline sample, changes its space group from *R3c* to *Pbnm*. All other samples belong to *R-3c* space group. *TEM* pictures show average sizes of 30 - 60 nm. Iodometry reveals oxygen excess for all samples.

4.2.3 Electrical properties of polycrystalline $La_{0.7}Ba_{0.3-x}Ca_xMnO_3$

Investigation in a four-point probe cryogenic system of polycrystalline samples revealed that all three substituted compounds exhibit a peak in electrical resistivity T_{p1} at around the same temperature of 226 K - 230 K. Lower values of resistivity support the result of the calculation of Mn^{3+} – O - Mn^{4+} angles and Mn – O bond length. Increase in the former and shortening of the latter would increase the "double exchange" metallic – ferromagnetic process, and the disorder introduced by the inclusion of Ca^{2+} spreads to the grain boundaries causing the phase separation.

All plots of ρ *vs* T show typical metal-insulator and *CMR* behavior. Magnetoresistivity (*MR*) is negative for all samples.

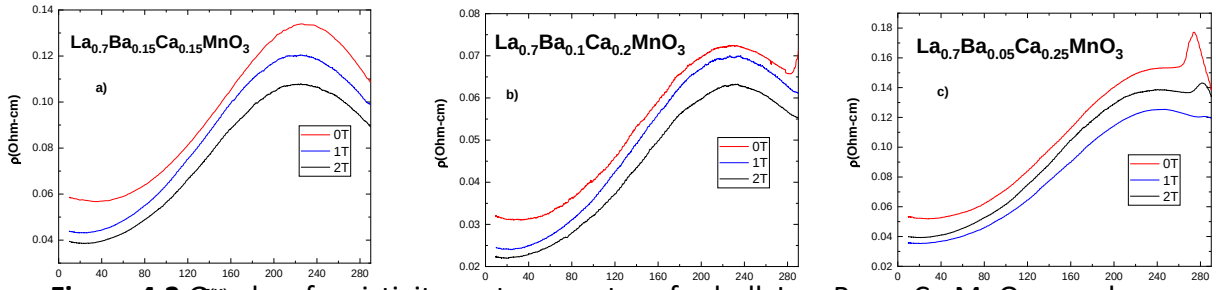

Figure 4.3 Graphs of resistivity vs. temperature for bulk $La_{0.7}Ba_{0.3-x}Ca_xMnO_3$ samples:

(a) x = 0.15, (b) x = 0.2, and (c) x = 0.25 [172].

Table 4.1 Experimental values for $La_{0.7}Ba_{0.3-x}Ca_xMnO_3$ bulk materials: electrical properties [172].

Compound (bulk)	T_C(K)	T_P(K)	ρ_{peak} (Ωcm) in 0 T	*MR*max (%) (1T)	*MR*max (%) (2T)	MR_{Max} (%) (1 T) at 10K	MR_{Max} (%) (2 T) at 10K
$La_{0.7}Ba_{0.3}MnO_3$	340	295	0.693	5.8	12.9	27.03	32.11
$La_{0.7}Ba_{0.15}Ca_{0.15}MnO_3$	308	226	0.134	10.18	19.72	25.12	32.59
$La_{0.7}Ba_{0.1}Ca_{0.2}MnO_3$	279	226	0.073	3.42	12.99	23.78	30.97
$La_{0.7}Ba_{0.05}Ca_{0.25}MnO_3$	261	230 (274T_{p2})	0.177	9.2 (22.04 T_{p2})	18.1 (31.94 T_{p2})	24.94	33.05

4.2.4. Magnetic properties of polycrystalline $La_{0.7}Ba_{0.3-x}Ca_xMnO_3$ compounds

Magnetic measurements in *ZFC-FC* regimes disclosed *FM/PM* behavior throughout the temperature range of 4 K – 360 K, for polycrystalline. The curves for the bulk samples show a sharp drop in magnetization at the transition. T_c for the bulk compound x = 0.15 shows the closest to the room temperature transition of 308 K. Further inclusion of Ca^+ ions to x = 0.2 leads to T_c = 279 K, also close to room temperature value. The last compound with x = 0.25 drops T_c to 261 K.

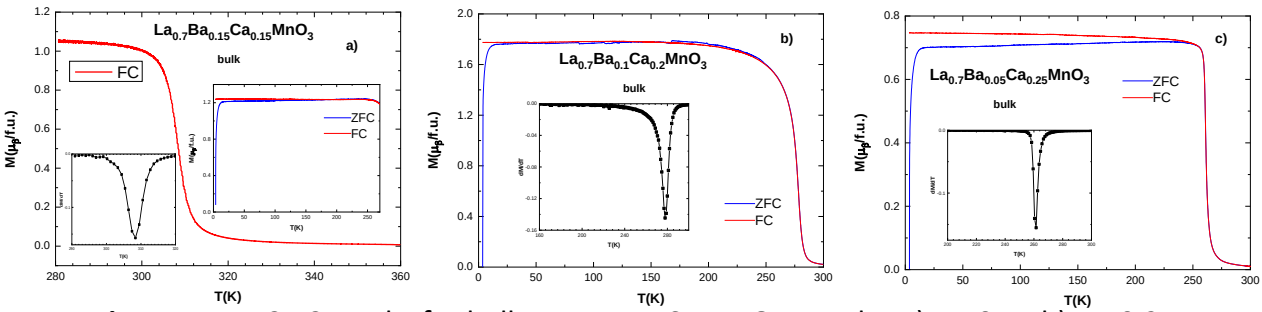

Figure 4.4 *ZFC-FC* graphs for bulk $La_{0.7}Ba_{0.3-x}Ca_xMnO_3$ samples a) x = 0.15 b) x = 0.2

c) x=0.25 [172].

4.2.5. Magnetic properties of nano-scale $La_{0.7}Ba_{0.3-x}Ca_xMnO_3$ compounds

The *ZFC-FC* magnetization measurements for nano-sized $La_{0.7}Ba_{0.3-x}Ca_xMnO_3$ particles show ferromagnetic behavior. The transition occurs more slowly than for the bulk compounds evidenced by the lower slope of the *ZFC-FC* curves. Derivatives of the plots with respect to temperature, shown in insets in Figure 4.5, reveal the value of transition temperature T_c. We see that this value is not as well defined as with the polycrystalline samples, particularly with x = 0.25 sample. Transition temperature drops with addition of Ca^{2+}. The compound with x = 0.15 exhibits T_c = 210 K, for x = 0.2: T_c = 185 K and for x = 0.25: T_c = 130 K.

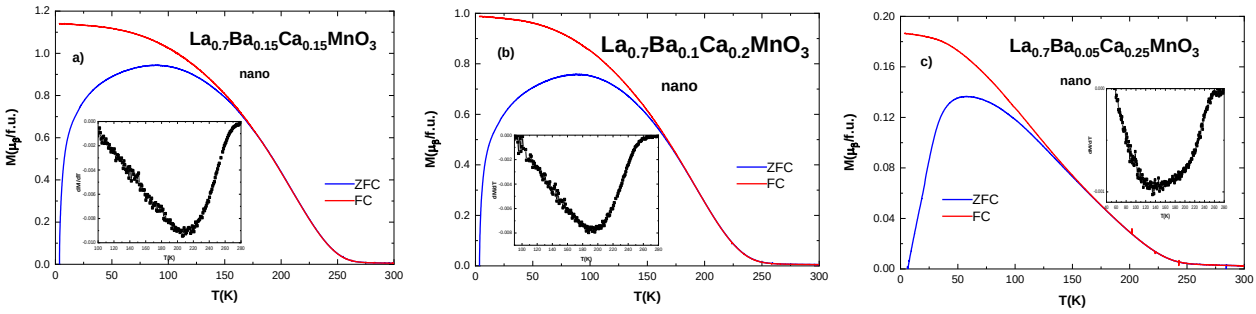

Figure 4.5 *ZFC-FC* graphs for nano $La_{0.7}Ba_{0.3-x}Ca_xMnO_3$ samples a) x = 0.15 b) x = 0.2 c) x = 0.25 [172].

4.2.6. Critical magnetic behavior of polycrystalline $La_{0.7}Ba_{0.3-x}Ca_xMnO_3$ samples

The positive slope of the Arrott plot curves confirms second-order transition for all samples. As an exception, the bulk compound x = 0.25 exhibits some anomalous behavior at higher, above T_c temperatures, with some semblance of a negative slope. This behavior comes as no surprise, as similar results have been reported in other studies on (La:Ca)MnO_3 compounds which do not show pure second order magnetic phase transitions [102].

Modified Arrott plot (*MAP*) method revealed the Tricritical mean-field model as the governing model for polycrystalline compounds. *MAP* method applied on the nano-sized compounds showed the same results as with the other nano-compounds in this study: they are governed by the mean-field model. These results, for $La_{0.7}Ba_{0.3-x}Ca_xMnO_3$ systems, were confirmed by Kouvel – Fisher (KF) method

Table 4.2 Critical exponent values for all $La_{0.7}Ba_{0.3-x}Ca_xMnO_3$ samples from the modified Arrott plot method [172].

Compound		γ	β	δ	T_c (K)
x= 0	bulk	1.065	0.288	4.69	340
x = 0.15	bulk	0.958	0.238	5.025	308
x = 0.2	bulk	0.979	0.245	4.996	279
x = 0.25	bulk	0.949	0.187	6.075	261
x = 0	nano	1.164	0.493	3.36	263
x= 0.15	nano	1.036	0.574	2.805	210
x = 0.2	nano	1.022	0.555	2.838	185
x = 0.25	nano	0.746	0.746	2	130
Mean-field model		1	0.5	3	
3D Heisenberg model		1.366	0.355	4.8	
Ising model		1.24	0.325	4.82	
Tricritical mean-field model		1	0.25	5	

4.2.8. Magnetic entropy change in polycrystalline $La_{0.7}Ba_{0.3-x}Ca_xMnO_3$ compounds

Graphs of $-\Delta S_m$ *vs* T in $\mu_0\Delta H$ = 1 T, 2 T, 3 T and 4 T, at temperature difference ΔT = 5 K show a higher peak and narrower curve for the bulk compounds, with the peak residing at T_c values. $|\Delta S_M|$ for the bulk samples exceeds the value for the parent compound. It increases for the samples with higher Ca^{2+} content. Existence of first-order-like transition presented in the sample with x = 0.25 further influences the entropy change. All maximum entropy change $|\Delta S_M|$ values at $\mu_\circ\Delta H$ = 1 T and $\mu_\circ\Delta H$ = 4 T are listed in the Table 4.3.

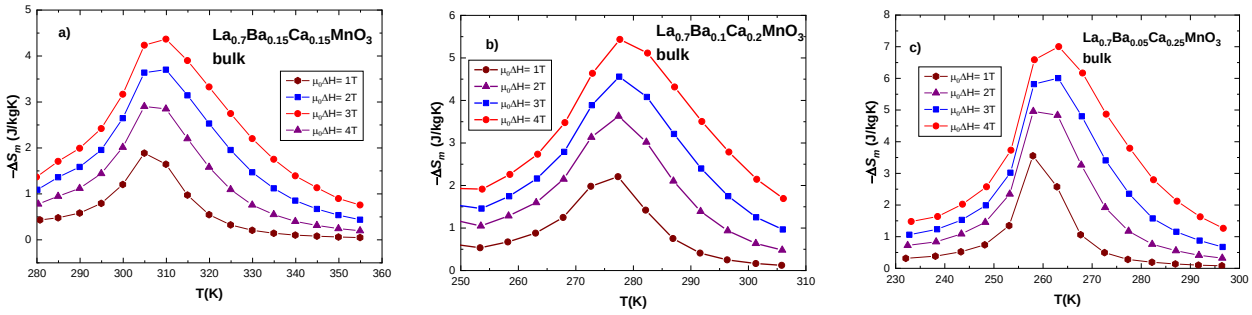

Figure 4.6 Magnetic entropy change vs temperature ($-\Delta S_M$ vs T) graphs for bulk $La_{0.7}Ba_{0.3-x}Ca_xMnO_3$ samples. a) x=0.15 b) x=0.2 c) x=0.1 d) x=0.25 [172].

4.2.9 Magnetic entropy change in nano-scale $La_{0.7}Ba_{0.3-x}Ca_xMnO_3$ compounds

Compared to the parent nano-compound $La_{0.7}Ba_{0.3}MnO_3$ the absolute value for entropy change $|\Delta S_M|$ in $\mu_o \Delta H$ = 1 T drops significantly for all Ca^+ including samples. For the parent compound $|\Delta S_M|$ = 1.04 J/KgK while for the x = 0.15 sample $|\Delta S_M|$ = 0.33 J/KgK. The x = 0.25 compound, as we saw in the section on hysteresis, *ZFC-FC* and Arrott plot observation, exhibits peculiar magnetization behavior and this directly influences its $|\Delta S_M|$ values. In $\mu_o \Delta H$ = 1 T it "only" reveals $|\Delta S_M|$ = 0.05 J/KgK.

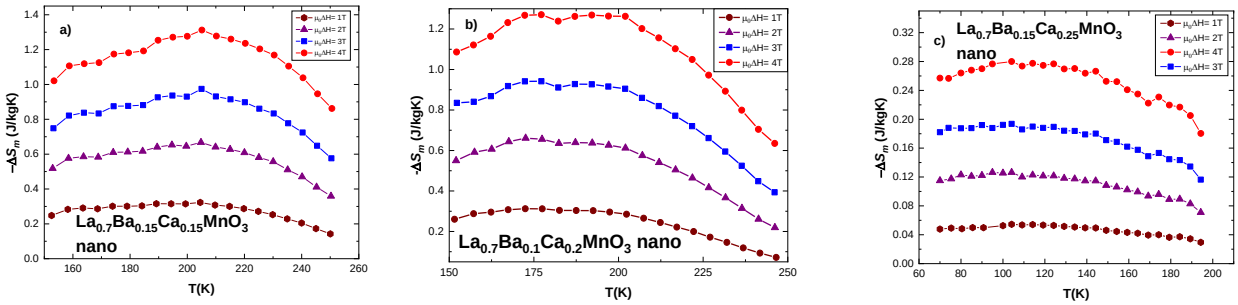

Figure 4.7 Magnetic entropy change vs temperature ($-\Delta S_M$ vs T) graphs for nano $La_{0.7}Ba_{0.3-x}Ca_xMnO_3$ samples a) x = 0.15 b) x = 0.2 c) x = 0.1 d) x = 0.25 [172].

4.2.10 Magnetocaloric effect in polycrystalline and nano-scale $La_{0.7}Ba_{0.3-x}Ca_xMnO_3$

RCP values for both systems are comparable in strength (except the nano-sample x = 0.25, showing lower values). In $\mu_0 \Delta H$ = 4 T, the curves for the bulk compounds widen increasing *RCP* values with respect to the parent compound. The values of *RCP* are presented in the table 4.3.

Table 4.3 Experimental values for $La_{0.7}Ba_{0.3-x}Ca_xMnO_3$ bulk and nano materials: magnetic measurements [172].

Compound	T_C (K)	M_s (μ_B/f.u.)	M_r (μ_B/f.u.)	M_r/M_s	H_{ci} (Oe)	$\lvert\Delta S_M\rvert$ (J/kgK) $\mu_0\Delta H$ = 1 T	$\lvert\Delta S_M\rvert$ (J/kgK) $\mu_0\Delta H$ = 4 T	*RCP* (*S*) (J/kg) $\mu_0\Delta H$ = 1 T	*RCP* (*S*) (J/kg) $\mu_0\Delta H$ = 4 T
$La_{0.7}Ba_{0.3}MnO_3$ (bulk)	340	4.04	0.24	0.06	200	1.33	3.5	53.7	158.4
$La_{0.7}Ba_{0.15}Ca_{0.15}MnO_3$	308	3.61	0.21	0.06	150	2.04	4.37	38.74	140.43
$La_{0.7}Ba_{0.1}Ca_{0.2}MnO_3$	279	3.68	0.54	0.15	110	2.29	5.43	41.26	184.69
$La_{0.7}Ba_{0.05}Ca_{0.25}MnO_3$	261	3.76	0.18	0.05	100	3.66	7.01	40.24	182.37
$La_{0.7}Ba_{0.3}MnO_3$ (nano)	263	2.79	1.16	0.41	480	1.04	1.37	105.4	130.1
$La_{0.7}Ba_{0.15}Ca_{0.15}MnO_3$	210	2.55	0.82	0.32	370	0.33	1.31	33.7	144.1
$La_{0.7}Ba_{0.1}Ca_{0.2}MnO_3$	185	2.39	0.73	0.31	440	0.32	1.28	35.2	153.6
$La_{0.7}Ba_{0.05}Ca_{0.25}MnO_3$	130		0.21		710	0.05	0.27	6.1	40.5

We estimated *TEC* in ΔT_{H-C} = 5 - 50 K and found that, for polycrystalline compounds, results are higher or similar to those for $La_{(0.7-x)}Eu_xBa_{0.3}MnO_3$ and $La_{(0.7-x)}Ho_xBa_{0.3}MnO_3$ compounds.

For the nano-scale compounds, the values of *TEC* is lower than for the bulk compounds (Figure 4.8).

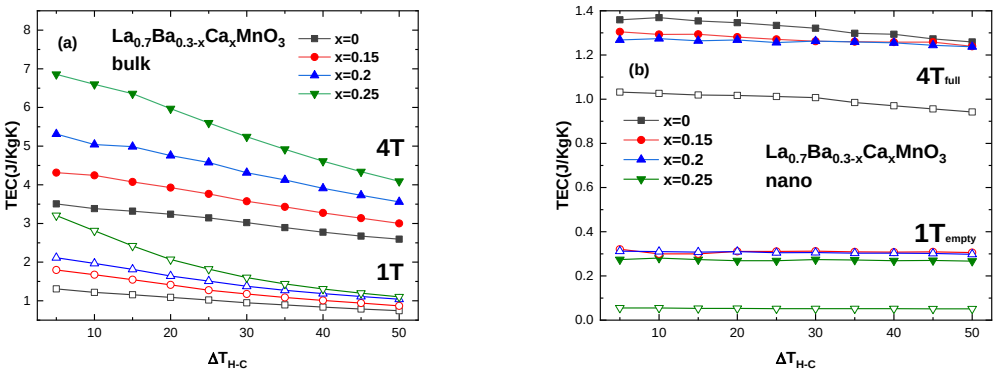

Figure 4.8 Temperature-averaged entropy change (*TEC*) for a) polycrystalline $La_{0.7}Ba_{0.15}Ca_{0.15}MnO_3$ b) nano-sized $La_{0.7}Ba_{0.15}Ca_{0.15}MnO_3$

Chapter 5. Structural analysis, electrical and magnetic properties, magnetoresistance, magnetocaloric effect in polycrystalline and nano-sized $Pr_{0.65}Sr_{0.35}MnO_3$ substituted with Ca.

5.1. Introduction

In this chapter, we will discuss another parent compound - $Pr_{0.65}Sr_{0.35}MnO_3$. Polycrystalline compounds $Pr_{1-x}Sr_xMnO_3$ has been studied before, reporting a variety of structural changes and phase transitions Our parent polycrystalline compound $Pr_{0.65}Sr_{0.35}MnO_3$ has been studied and reported before by F. Guillou at al in 2012 [74]. Its phase transition, electrical and magnetic properties revealed T_c = 295K and second order *FM*/*PM* magnetic transition with relatively high magnetocaloc effect as well as a metal – insulator transition associated with *FM/PM* structure. Additionally, Ajay Kumar Saw at al, have reported studies on $Pr_{0.67}Sr_{0.33}MnO_3$ assigning it magnetic and electrical properties similar to $Pr_{0.65}Sr_{0.35}MnO_3$ and adding structural studies, giving it a *Pbnm* space group [99]. To our knowledge, no investigations have been made on nano-scaled $Pr_{0.65}Sr_{0.35}MnO_3$ compounds, leading to us synthesizing and investigating our own.

5.3. Results and discussion

5.3.1 Structural characterization of polycrystalline $Pr_{0.65}Sr_{0.35-x}Ca_xMnO_3$ (x = 0.02, 0.05, 0.1, 0.2, 0.3)

Rietveld refinement analysis showed best fit results for orthorhombic structure in the space group *pbnm* (62) for all bulk samples. Lattice dimensions and cell volume for x = 0.05 compound are larger than for the x = 0.02 compound, against expectations, and then become smaller for every subsequent sample.

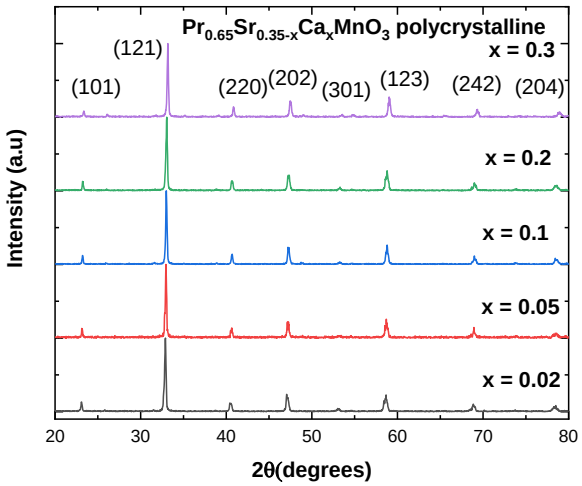

Figure 5.1 X-ray diffraction patterns for $Pr_{0.65}Sr_{0.35-x}Ca_xMnO_3$ polycrystalline samples [183]

Oxygen stoichiometry investigation, done through Iodometric analysis, uncovered low oxygen deficiency for the bulk samples.

5.3.2 Structural characterization of nano-scale $Pr_{0.65}Sr_{0.35-x}Ca_xMnO_3$ (x = 0.02, 0.05, 0.1, 0.2, 0.3)

Akin to the polycrystalline samples, no extraordinary additional peaks are observed, as can be seen in the figure 5.3. All peaks are generally wider than the peaks for the bulk samples and they belong to Orthorhombic reflection planes in the '*pbnm*' space group. This is confirmed by Rietveld refinement analysis.

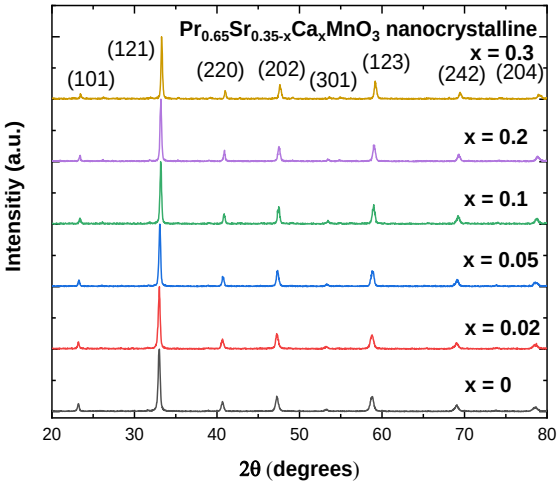

Figure 5.2 X-ray diffraction patterns for $Pr_{0.65}Sr_{0.35-x}Ca_xMnO_3$ nanocrystalline samples [184]

Calculations of the bond length Mn – O and angle Mn^{3+} – O – Mn^{4+} using the results of Rietveld refinement, show that the bond length becomes shorter as the substitution grows. Iodometric titration performed on the nano-scale particles gave similar results obtained on other systems (table 5.6), in particular, it revealed modest oxygen excess. All samples exhibit an average oxygen stoichiometry of $O_{3.01-3.02}$ within a reliable error range.

5.3.3 Electrical properties of polycrystalline $Pr_{0.65}Sr_{0.35-x}Ca_xMnO_3$

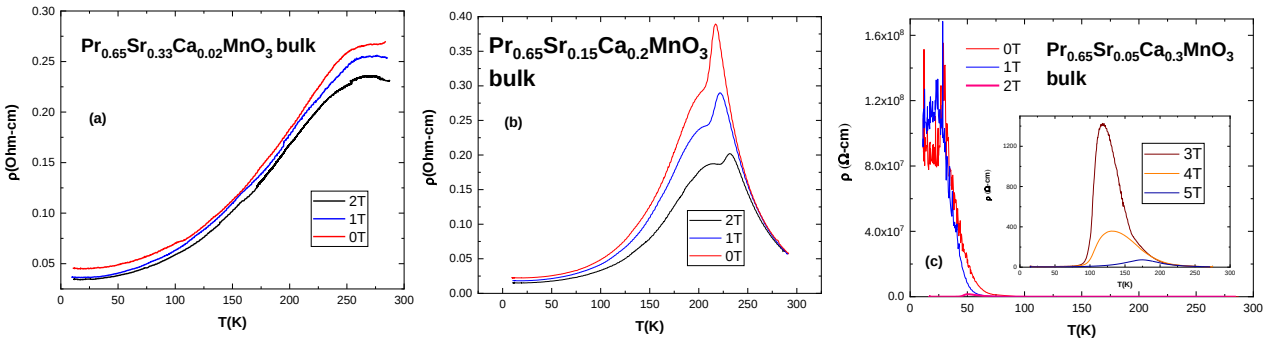

Figure 5.3 Graphs of resistivity vs. temperature for bulk $Pr_{0.65}Sr_{0.35-x}Ca_xMnO_3$ samples:

(a) x = 0.02, (b) x = 0.2, (c) x = 0.3; The inset shows plot of resistivity at higher fields which are not visible in the main plot [184].

Measurements of resistivity of the polycrystalline compounds in four-point probe cryogenic system uncovered typical *CMR* behavior for the samples x = 0.02, 0.5, 0.1 and 0.2. We saw that samples with lower Ca^{2+} content exhibit one single peak in resistivity, designated T_{p1}, associated with the dominance of the grain boundaries. Starting with the sample x = 0.1, a higher, sharper peak begins to be visible at higher temperatures but it remained beyond the temperature range until the x = 0.2 sample. This peak, resulting from the *FM-PM* transition is higher in resistivity than the peak caused by the grain boundaries and exhibits greater magnetoresistance (*MR*). In addition, the peak is shifted to higher temperatures under external field due to lowered spin fluctuations and electron localization.

Resistance for the x = 0.3 bulk sample was beyond detection at temperatures below 80 K in $\mu_{\circ}H$ = 0 T, 1 T. With application of stronger field, 2T, the resistance dropped significantly and was within the detection limit of the apparatus. In higher field of $\mu_{\circ}H$ = 3 T, 4 T, 5 T, the curve lowered progressively and shifted to higher temperature range. This behavior indicated that intergrain properties are dominant in the sample and the external field aligns the spins promoting electron tunneling – behavior characteristic of *CMR*.

Table 5.1 Experimental values for $Pr_{0.65}Sr_{0.35-x}Ca_xMnO_3$ bulk materials: electrical properties [184].

Compound (Bulk)	T_C **(K)**	T_{P1} **(K)** (T_{P2} **(K))**	ρ_{peak} **(Ωcm) in 0 T**	MR_{Max} **(%) (1 T)**	MR_{Max} **(%) (2 T)**
$Pr_{0.65}Sr_{0.33}Ca_{0.02}MnO_3$	273	274	0.285	4.45	11.99
$Pr_{0.65}Sr_{0.3}Ca_{0.05}MnO_3$	261	273	0.339	12.28	22.75
$Pr_{0.65}Sr_{0.25}Ca_{0.1}MnO_3$	244	256 (258)	0.199	23.28	33.27
$Pr_{0.65}Sr_{0.15}Ca_{0.2}MnO_3$	201	210 (217)	0.389	29.08	51.96
$Pr_{0.65}Sr_{0.05}Ca_{0.3}MnO_3$		-	$>100 \times 10^8$ (72.985 in 5 T)	77.62 (between 3 and 4 T)	99.99 (between 2 and 3 T)

5.3.4 Magnetic properties of polycrystalline $Pr_{0.65}Sr_{0.35-x}Ca_xMnO_3$ compounds

Magnetic measurements in field cooled and zero field cooled (ZFC-FC, $\mu_{\circ}H$= 0.05 T) environment and temperature range of 4 - 300 K showed typical ferromagnetic curves for all compounds, excluding x = 0.3 samples. As expected, samples with higher Ca^{2+} content exhibited lower T_c than the preceding sample. Polycrystalline compounds exhibited high T_c values than their nano-sized counterparts. First sample x = 0.02 lowers T_c from 295 K for the parent compound to 273 K. For x = 0.2, it is lowered to 201 K.

X = 0.3 samples exhibits different *ZFC-FC* curves. It manifests multiple transitions throughout the temperature range. At around 210 – 215 K, the sample shows *CO* transition characterized by increase in magnetization (CO-AFM). Further down in temperature, at around 150 - 170 K the bulk compound enters a *AFM* state (CE-AFM). At lower temperatures, the *ZFC-FC* curves show

an increase in magnetization, affiliated with formation of *FM c*lusters among the *AFM* matrix with spin-glass-like behavior.

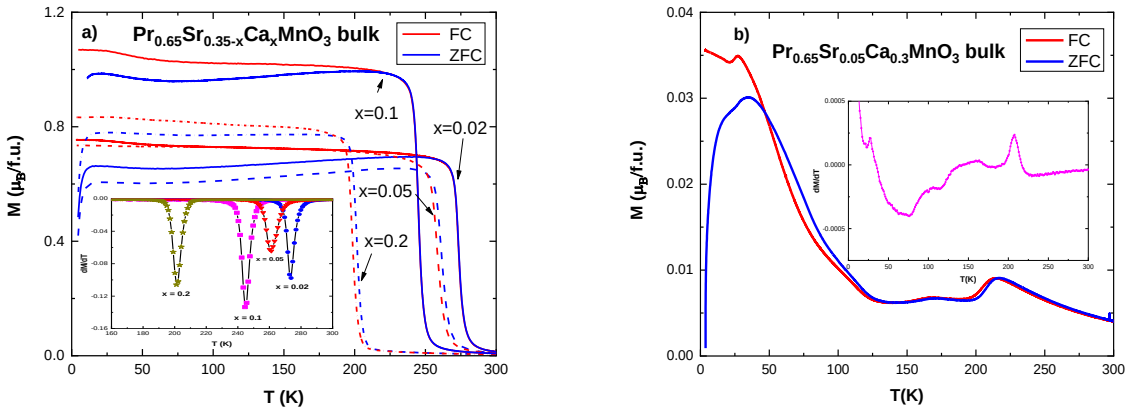

Figure 5.4 *ZFC-FC* graphs for bulk $Pr_{0.65}Sr_{0.35-x}Ca_xMnO_3$ samples a) x = 0.02, 0.05, 0.1, 0.2 b) 0.3 [184].

5.3.5 Magnetic properties of nano-scale $Pr_{0.65}Sr_{0.35-x}Ca_xMnO_3$ compounds

ZFC-FC curves for nano-scale samples show lower slope at the transition than for the polycrystalline compounds, but not as low as for some other nano-scale systems studied in this work. This suggests, a larger size (and Curie temperature) distribution. The low temperature increase in magnetization observed in the bulk compounds and associated with Pr^{3+} magnetization is not easily visually observable in the nano-compounds.

The sample x = 0.3, whose *ZFC – FC* curves are shown in 5.8b, exhibits similar behavior to its bulk counterpart. Its *CO* formation at around 210 K is not as pronounced and the transition to the *AFM* state is not easily distinguishable. Rise in magnetization associated with the formation of *FM* clusters occurs at higher temperatures compared to the bulk sample, at 150 K. There is also no visible feature at 35 K caused by spin blocking between *FM* clusters.

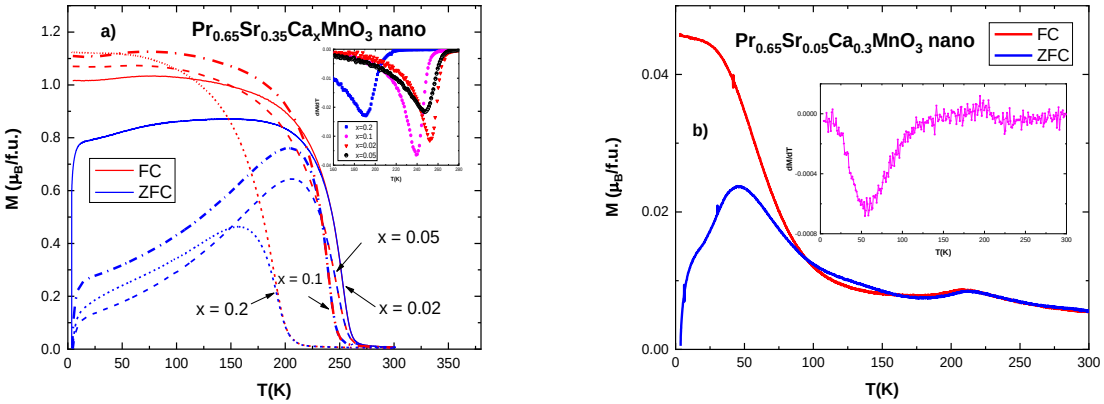

Figure 5.5 *ZFC-FC* graphs for nano $Pr_{0.65}Sr_{0.35-x}Ca_xMnO_3$ samples a) x = 0.02, 0.05, 0.1, 0.2 b) 0.3 [184].

5.3.6 Critical magnetic behavior of polycrystalline $Pr_{0.65}Sr_{0.35-x}Ca_xMnO_3$ samples

Table 5.2 Critical exponent values for all $Pr_{0.65}Sr_{0.35-x}Ca_xMnO_3$ samples from modified Arott plot method [184].

Compound		γ	β	δ	T_c (K)
x = 0.02	bulk	1.057	0.212	5.986	273
x = 0.05	bulk	0.981	0.232	5.228	261
x = 0.1	bulk	0.985	0.25	4.94	244
x = 0.2	bulk	-	-	-	201
x = 0.3	bulk	-	-	-	-
x = 0	nano	0.895	0.521	2.72	255
x= 0.02	nano	0.997	0.508	2.96	252
x = 0.05	nano	0.962	0.523	2.84	249
x = 0.1	nano	1.015	0.602	2.68	239
x = 0.2	nano	-	-	-	191
x = 0.3	nano	-	-	-	-
Mean field model		1	0.5	3	
3D Heisenberg model		1.366	0.355	4.8	
Ising model		1.24	0.325	4.82	
Tricritical mean field model		1	0.25	5	

Arrott plot for the bulk x = 0.3 sample at 150 – 230 K reveals a magnetic ordering change at 215 K. At 25 K – 125 K, the lines show strong competition between *FM* and *AFM* ordering. For the x = 0.3 nano-sample, at 170 K to 260 K, the change occurs at 215 K. Arrott plot at low temperatures 30 - 130 K, discloses stronger *FM* presence.

For all bulk compounds, critical exponents were discovered to belong to the tricritical mean-free model, akin to other polycrystalline samples in this work. For the nano-scale compounds, the exponents can claim to belong to mean field model, albeit diverging slightly from the nominal values.

5.3.8 Magnetic entropy change in polycrystalline $Pr_{0.65}Sr_{0.35-x}Ca_xMnO_3$ compounds

All samples exhibit negative entropy change ($-\Delta S_m$) except for both x = 0.3 samples in the 150 - 230 K range. Polycrystalline compounds show large absolute entropy change $|\Delta S_M|$, compared to many other manganites. High results were expected based on some reports on the entropy change in other Pr^{3+} and Ca^{2+} based manganite.

We investigated ΔS_M for x = 0.3 sample at two different temperature ranges. Illustrated in figure 5.14e, entropy change is positive at around 200 - 210 K, concurrent with expectations from an *CO-AFM* ordering. At slightly higher temperatures, higher than 210 K, entropy change is negative, albeit not large, suggesting some *PM* transition supported by the *ZFC-FC* graph. We should also note positive ΔS_M at around 160K, suggesting the formation of *AFM* state. Positive entropy change is normally not as high as negative entropy change, but it usually occurs at wider temperature range and can be implemented in combination with "normal" entropy change material to enhance *MCE* [76, 78, 79, 190].

From 5.14f, calculations for x = 0.3 at around 35 - 40 K discloses very large ΔS_M. At $\mu_0\Delta H$ = 1 T, the change is 4.6 J/KgK, and at $\mu_0\Delta H$ = 4 T it is 15.3 J/KgK. Such large ΔS_M should make the compound as a viable candidate in cryogenics. All values of $|\Delta S_M|$ in fields $\mu_0\Delta H$ = 1 T, 4 T are listed in the table 5.3.

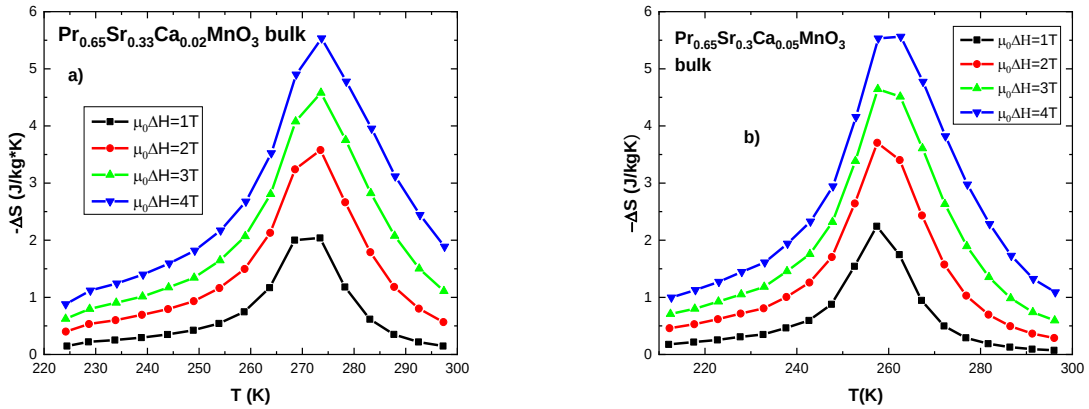

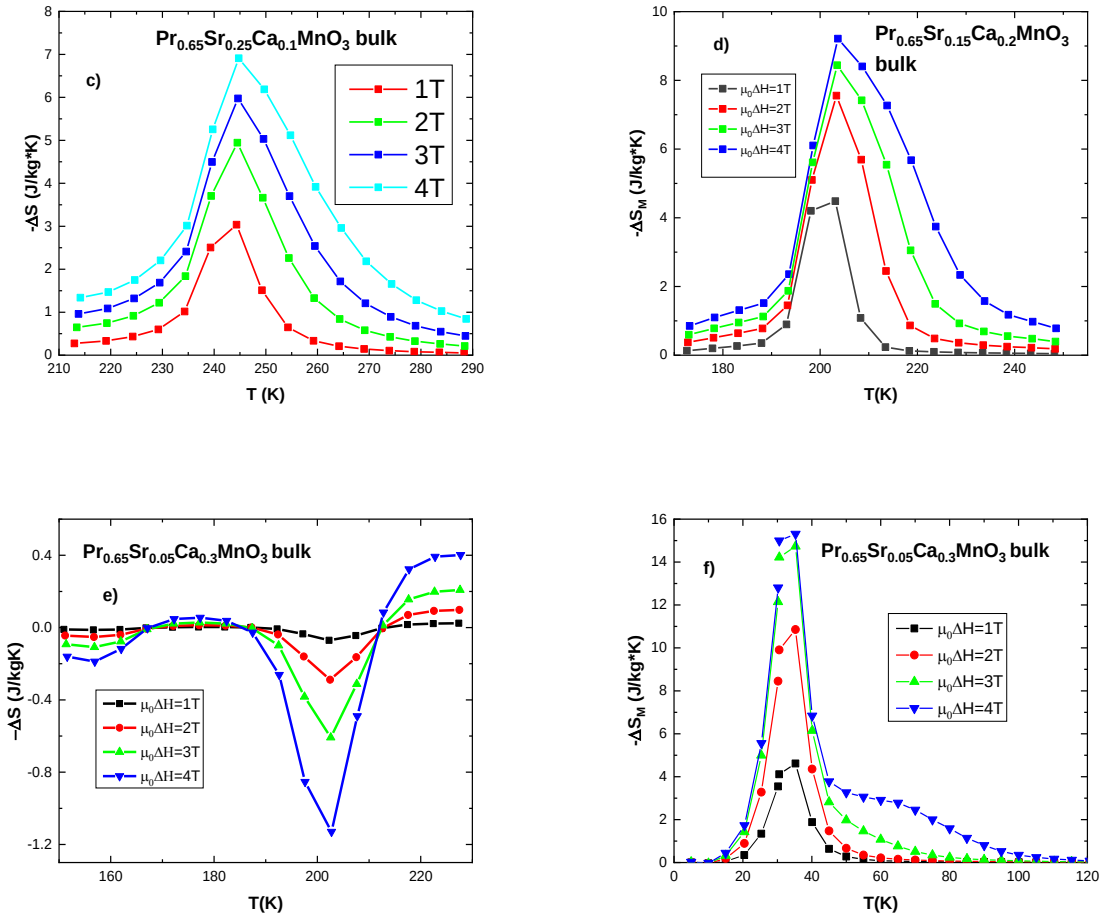

Figure 5.6 Magnetic entropy change vs temperature ($-\Delta S_M$ vs T) graphs for bulk $Pr_{0.65}Sr_{0.35-x}Ca_xMnO_3$ samples. a) x=0.02 b) x=0.05 c) x=0.1 d) x=0.2 e) x = 0.3 at 205 K f) x = 0.3 at 40 K [184]

5.3.9 Magnetic entropy change in nano-scale $Pr_{0.65}Sr_{0.35-x}Ca_xMnO_3$ compounds

Nano-scale compounds exhibited lower values of entropy change than bulk compounds but are nonetheless equal or even higher than the entropy change found in other manganites.

Nano x = 0.3 sample exhibits high entropy change at low temperatures of 75 K.

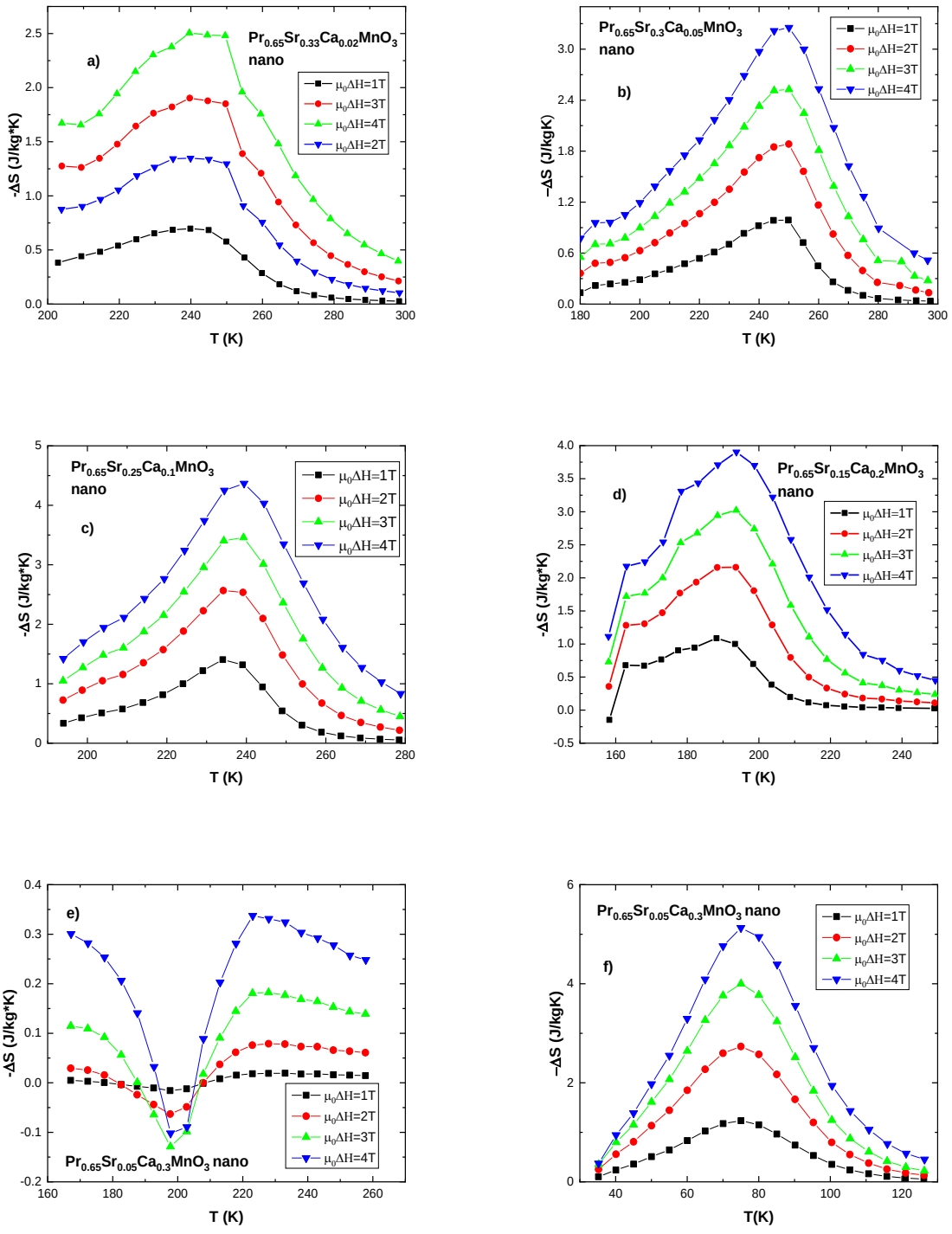

Figure 5.7 Magnetic entropy change vs temperature ($-\Delta S_M$ vs T) graphs for nano-scale $Pr_{0.65}Sr_{0.35-x}Ca_xMnO_3$ samples. a) x=0.02 b) x=0.05 c) x=0.1 d) x=0.2 e) x = 0.3 at 205 K f) x = 0.3 at 75 K [184].

5.3.10 Magnetocaloric effect in polycrystalline and nano-scale

$Pr_{0.65}Sr_{0.35-x}Ca_xMnO_3$

Although there is no report on the exact value of *RCP* for the bulk parent compound, it is estimated to be in 45 J/Kg – 55 J/Kg range in $\mu_0\Delta H$ = 1 T. The bulk x = 0.02 sample exhibits lower *RCP* but subsequent samples increase their *RCP*.

Nano-scale compounds make up for their lower values for absolute entropy change by having wider temperature range δT_{FWHM}, and so, their *RCP* values similar to the values of the bulk compounds.

Table 5.3 Experimental values for $Pr_{0.65}Sr_{0.35-x}Ca_xMnO_3$ materials: magnetic measurements [184].

Compound	T_C (K)	M_s (μ_B/f.u.)	M_r (μ_B/f.u.)	M_r/M_s	H_{ci} (Oe)	$\lvert\Delta S_M\rvert$ (J/kgK) $\mu_0\Delta H$ = 1 T	$\lvert\Delta S_M\rvert$ (J/kgK) $\mu_0\Delta H$ = 4 T	RCP (*S*) (J/kg) $\mu_0\Delta H$ = 1 T	RCP (*S*) (J/kg) $\mu_0\Delta H$ = 4 T
$Pr_{0.65}Sr_{0.35}MnO_3$ (bulk) [74]	295					2.3			
$Pr_{0.65}Sr_{0.33}Ca_{0.02}MnO_3$	273	3.71	0.33	0.09	180	2.04	5.53	34	166
$Pr_{0.65}Sr_{0.3}Ca_{0.05}MnO_3$	261	3.78	0.37	0.1	170	2.24	5.56	44	167
$Pr_{0.65}Sr_{0.25}Ca_{0.1}MnO_3$	244	3.94	0.41	0.1	190	3.03	6.91	45	186
$Pr_{0.65}Sr_{0.15}Ca_{0.2}MnO_3$	201	3.97	0.28	0.07	160	4.48	9.21	60	270
$Pr_{0.65}Sr_{0.05}Ca_{0.3}MnO_3$		3.81	0.27	0.7	170	4.6 (40 K)	15.3 (40 K)	92 (40 K)	380 (40 K)
$Pr_{0.65}Sr_{0.35}MnO_3$ (nano)	255	2.95	1.14	0.39	810	0.54	2.05	24	102
$Pr_{0.65}Sr_{0.33}Ca_{0.02}MnO_3$	252	3.08	1.11	0.36	720	0.69	2.5	38	175
$Pr_{0.65}Sr_{0.3}Ca_{0.05}MnO_3$	249	3.16	1.16	0.37	540	0.99	3.25	48	178
$Pr_{0.65}Sr_{0.25}Ca_{0.1}MnO_3$	239	3.49	1.13	0.32	510	1.41	4.37	39	215
$Pr_{0.65}Sr_{0.15}Ca_{0.2}MnO_3$	191	3.39	1.07	0.31	620	1.08	3.9	41	185
$Pr_{0.65}Sr_{0.05}Ca_{0.3}MnO_3$		-			600	1.23(75 K)	5.12(75 K)	48(75 K)	204(75 K)

TEC calculations reveal similar leaders to *RCP* in cooling potential. Bulk compounds reveal very high values.

Nano-scale samples reveal lower *TEC* values, but are on par with some bulk compounds found in literature and in this work.

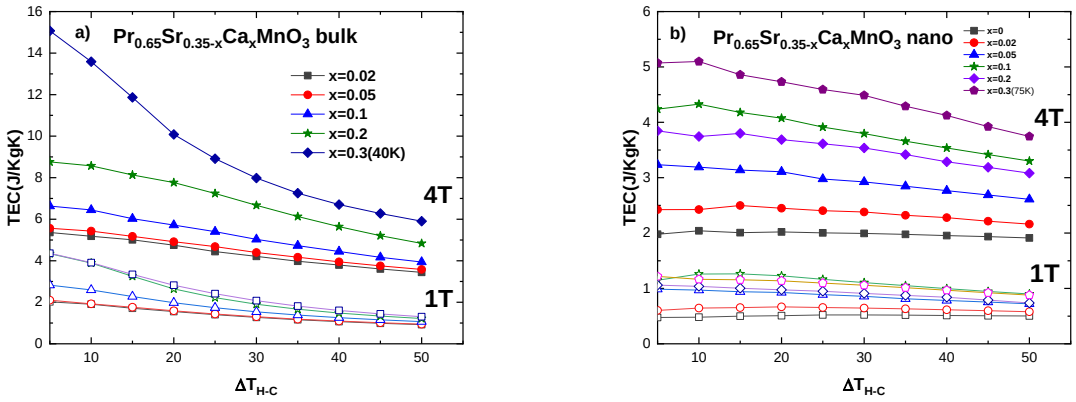

Figure 5.8. Temperature-averaged entropy change (TEC) vs ΔT_{H-C} for a) polycrystalline $Pr_{0.65}Sr_{0.35-x}Ca_xMnO_3$ b) nano-sized $Pr_{0.65}Sr_{0.35-x}Ca_xMnO_3$ [184].

Chapter 6. Structural analysis, electrical and magnetic properties, magnetocaloric effect in polycrystalline and nano-sized $Pr_{0.65}Sr_{0.35}MnO_3$ substituted with Nd.

6.1 Introduction

In this chapter, we will continue the investigation on the parent compound $Pr_{0.65}Sr_{.35}MnO_3$ by substitution on the A-site with a smaller ionic size Nd^{3+} ions (x = 0.05, 0.15, 0.25, 0.35). Nd^{3+}-ions (1.163 Å) are smaller than both Pr^{3+} (1.179 Å) and Sr^{2+} (1.31 Å) ions as well as the Ca^{2+} (1.18 Å) ions used for substitution in the previous chapter, thus we expect further change in structural properties. Such changes could potentially affect electrical and magnetic properties, including lower T_c and increased magnetocaloric effect.

6.2 Results and discussion

6.2.1 Structural characterization of polycrystalline $Pr_{0.65-x}Nd_xSr_{0.35}MnO_3$ (x = 0.05, 0.15, 0.25, 0.35)

The parent compound's series $Pr_{0.65-x}Sr_xMnO_3$ has been studied to exhibit orthorhombic structure in "*Pbnm*" space group symmetry. Polycrystalline samples switched to *R-3c* symmetry beginning with x = 0.15 substitution level. After the change, lattice parameters and cell volume decrease with

the increase of smaller Nd^{3+} ions. The lattice parameters and the cell volume diminish with increasing Nd^{3+} - ion content as they have smaller ionic radius than the Pr^{3+} - ions.

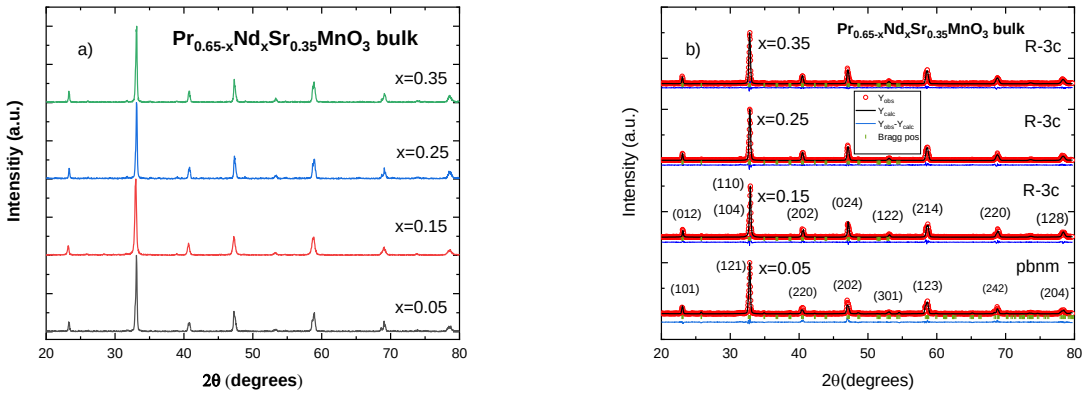

Figure 6.1 a) X-ray diffraction patterns for $Pr_{0.65-x}Nd_xSr_{.35}MnO_3$ polycrystalline samples b) best-fit results using Rietveld refinement method [191].

Implementation of Iodometric titration analysis demonstrated oxygen deficiency for all polycrystalline compounds, as could be expected based on the results from previous analysis on the other systems. An average of $O_{2.94\ -\ 2.97}$ was calculated with a relative standard deviation not exceeding a value of 2, making the results reliable.

6.2.2 Structural characterization of nano-scale $Pr_{0.65-x}Nd_xSr_{0.35}MnO_3$ compounds (x = 0.05, 0.15, 0.25, 0.35)

X – ray diffraction patterns for nano-scale $Pr_{0.65-x}Nd_xSr0_{.35}MnO_3$ samples displayed in Figure 6.2a exhibit wider peaks than their polycrystalline counterparts based on their smaller crystallite sizes. Like with the bulk compounds, there is a slight shift to smaller reflection angles for the x = 0.15 compound suggesting a structural change. Rietveld refinement analysis confirms a change from Orthorhombic for x = 0, 0.05 compounds to Rhombohedral structure for all others. Figure 6.2b presents best-fit results from Rietveld analysis showing a good fit for all compounds.

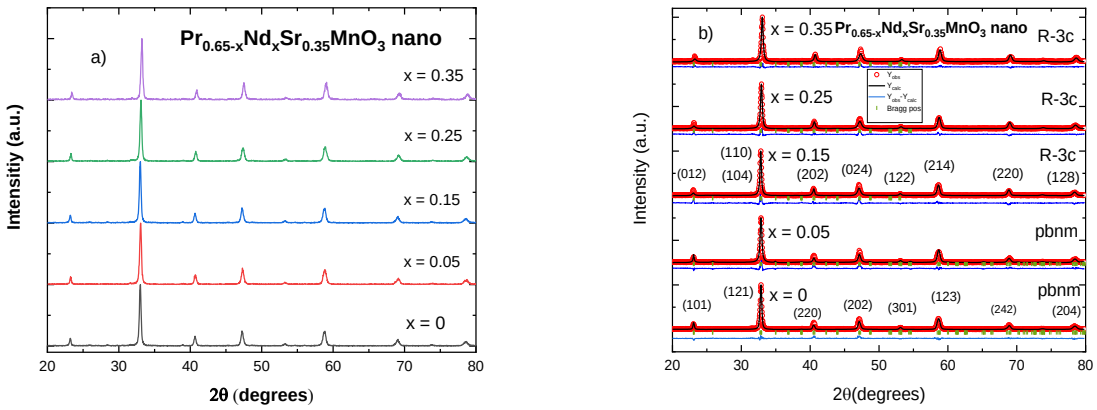

Figure 6.2 a) X-ray diffraction patterns for $Pr_{0.65-x}Nd_xSr_{0.35}MnO_3$ nano-scale samples b) best fit results using Rietveld refinement method [191].

Iodometric analysis of the Mn^{3+}/Mn^{4+} ratio demonstrated an excess of Mn^{4+} ions resulting in an oxygen excess in the compound's stoichiometry.

6.2.3 Electrical properties of polycrystalline $Pr_{0.65-x}Nd_xSr_{0.35}MnO_3$

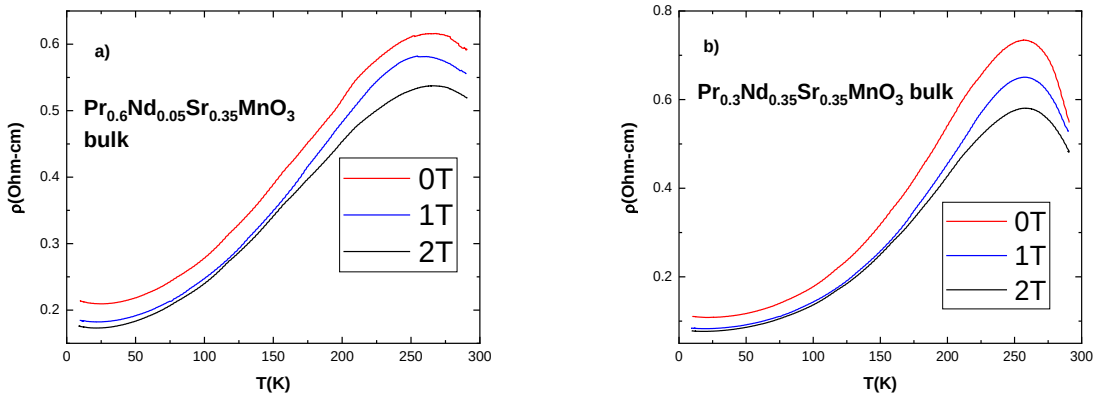

Figure 6.3 Graphs of resistivity vs. temperature for bulk $Pr_{0.65-x}Nd_xSr_{0.35}MnO_3$ samples under μ_0H = 0 T, 1 T and 2 T: (a) x = 0.05, (b) x = 0.35 [191]

Electrical properties of the polycrystalline samples were in the temperature range 10 – 290 K and in external fields $\mu_0 H$ = 0 T, 1 T, 2 T. All samples exhibit typical *CMR* behavior. Every sample exhibited a single peak in the ρ vs T graphs. This peak, T_{p1}, is associated with magnetic transition T_c and with grain boundaries. All values of T_{p1} lie below those of T_c.

At very low temperatures a very small increase in resistivity is observed after a minimum which is attributed to inter and intra-grain effects

Maximum resistivity ρ_{max} values are larger than those recorded for $Pr_{0.65}Sr_{0.35-x}Ca_xMnO_3$ compounds, suggesting larger grain boundary role. *MR* is negative for all samples.

Table 6.1 Experimental values for bulk $Pr_{0.65-x}Nd_xSr_{0.35}MnO_3$ materials: electrical properties [191].

Compound (Bulk)	T_C **(K)**	T_{P1} **(K)**	ρ_{peak} **(Ωcm) in 0 T**	MR_{Max} **(%) (1 T)**	MR_{Max} **(%) (2 T)**
$Pr_{0.6}Nd_{0.05}Sr_{0.35}MnO_3$	284	266	0.616	6	12.82
$Pr_{0.5}Nd_{0.15}Sr_{0.35}MnO_3$	279	261	0.846	6.74	14.54
$Pr_{0.4}Nd_{0.25}Sr_{0.35}MnO_3$	271	265	1.275	5.88	14.12
$Pr_{0.3}Nd_{0.35}Sr_{0.35}MnO_3$	268	257	0.734	11.44	20.98

6.2.4 Magnetic properties of polycrystalline $Pr_{0.65-x}Nd_xSr_{0.35}MnO_3$ compounds

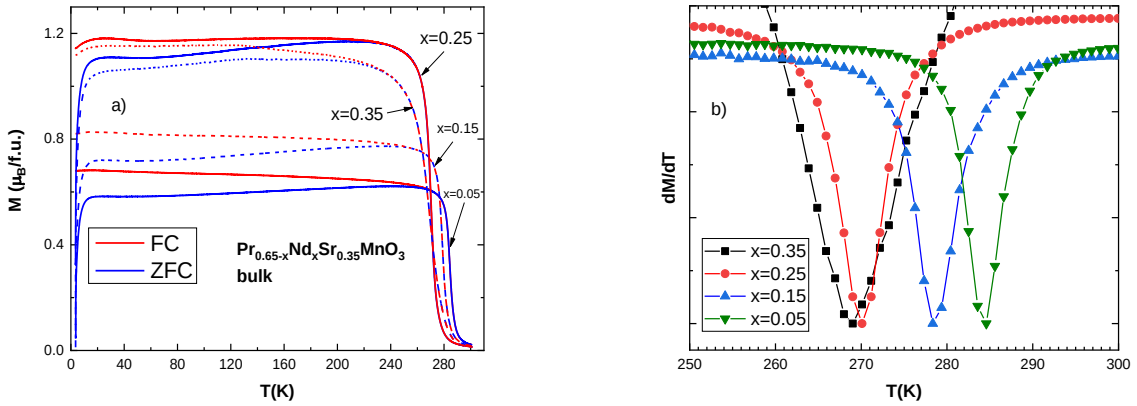

Figure 6.4 a) *ZFC-FC* curves and b) derivative of magnetization for bulk $Pr_{0.65-x}Nd_xSr_{0.35}MnO_3$ samples [191].

The *ZFC-FC* magnetization measurements in a field of $\mu_0 H$ = 0.05 T of the bulk samples reveal *FM/PM* transition for all samples. In Figure 6.4a, a sharp drop in magnetization is noted for each sample as the samples undergo a transition from *FM* to *PM* state. A derivative of the curves shows a minimum at the inflection of the magnetization drop and represents T_c. In Figure 6.4b we see that the values for Curie temperature drop for higher Nd^{3+} ions content samples, from 295 K [74] for the parent compound, to 284 K for the x = 0.05 sample and to 279 K for the x = 0.15 sample. Lowering of T_c is not as drastic as for other compounds in this work, for example for $Pr_{0.65}Sr_{0.35-x}Ca_xMnO_3$ compounds, due to Nd^{3+} being closer to Pr^{3+} ionic radius (1.163 Å and

1.179 Å in 9 coordination) than Ca^{2+} to Sr^{2+} radius (1.18 Å and 1.31 Å). In fact, the difference between the T_c values of the samples with x = 0.25 and x = 0.35 is only 3 K. This result means that any substitution of the parent compound with Nd^{+} ions in the range 0 < x < 0.35 will produce compounds with near room temperature transition.

6.2.5 Magnetic properties of nano-scale $Pr_{0.65-x}Nd_xSr_{0.35}MnO_3$ compounds

Comparing *ZFC-FC* curves to their bulk counterparts, the first obvious observation to be made is that the transition from *FM* to *PM* states occurs at a wider temperature range, i.e. the slope is lower. Sample x= 0.05 lowers T_c from 255 K for the parent compound to 251 K. The sample x = 0.15 lowers it further to 246 K, and for x = 0.25 and x = 0.35 showing minimum at 229 K and 224 K, respectively.

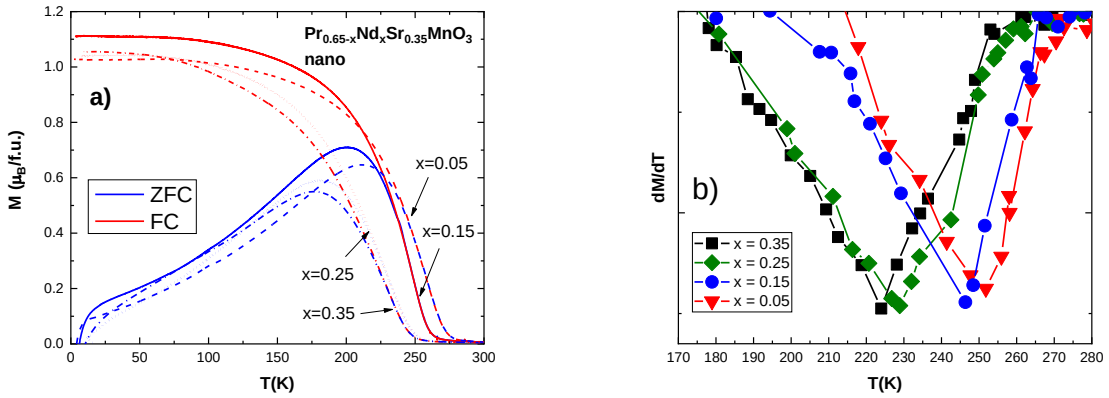

Figure 6.5 a) *ZFC-FC* curves and b) derivative of magnetization for nano-scale $Pr_{0.65-x}Nd_xSr_{0.35}MnO_3$ samples [191].

6.2.6 Critical magnetic behavior of polycrystalline $Pr_{0.65-x}Nd_xSr_{0.35}MnO_3$ samples

Arrott plots, reveal only second-order magnetic phase transitions for all samples, based on the positive slope of the curves. Modified Arrott plot (*MAP*) method was implemented in order to find true critical exponents β, γ and δ. For bulk compounds, samples x = 0.05 and x = 0.15 were found to be governed by the tricritical mean field model. For the other two, x = 0.25 and x = 0.35 samples the exponent β diverged from the tricritical value of 0.25 and was found to be closer to 3D Heisenberg model's 0.355. For nano-scale compounds, all exponents were found to lie in the mean-field model's values for long-range interactions, just as for all other nano-scale compounds under investigation in this study.

Table 6.2 Critical exponent values for all samples $Pr_{0.65-x}Nd_xSr_{0.35}MnO_3$ from modified Arott plot method [191].

Compound		γ	β	δ	T_c (K)
x = 0.05	bulk	0.99	0.247	5.01	284
x = 0.15	bulk	0.878	0.297	3.96	279
x = 0.25	bulk	0.911	0.377	3.42	271
x = 0.35	bulk	0.993	0.385	3.58	268
x = 0	nano	0.895	0.521	2.72	255
x = 0.05	nano	0.905	0.509	2.78	251
x = 0.15	nano	0.897	0.512	2.75	246
x = 0.25	nano	0.911	0.503	2.81	229
x = 0.35	nano	0.915	0.516	2.77	224
Mean field model		1	0.5	3	
3D Heisenberg model		1.366	0.355	4.8	
Ising model		1.24	0.325	4.82	
Tricritical mean field model		1	0.25	5	

6.2.8 Magnetic entropy change in polycrystalline $Pr_{0.65-x}Nd_xSr_{0.35}MnO_3$ compounds

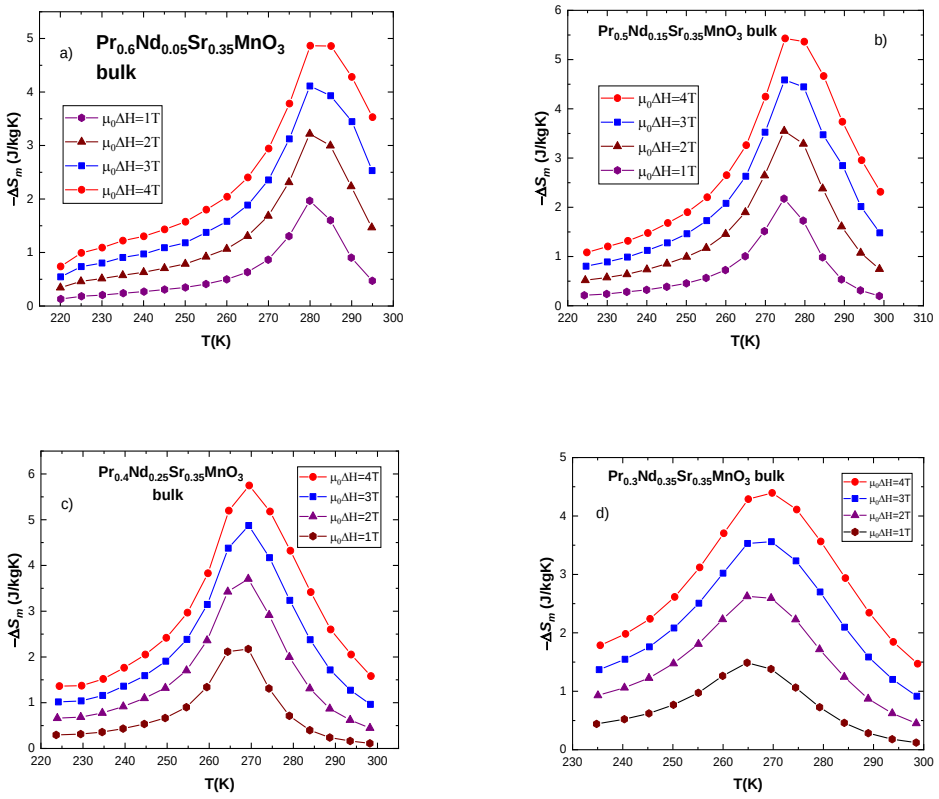

Figure 6.6 Magnetic entropy change vs temperature ($-\Delta S_M$ vs T) graphs for bulk $Pr_{0.65-x}Nd_xSr_{0.35}MnO_3$ samples. a) x=0.05 b) x=0.15 c) x=0.25 d) x=0.35 [191].

Maximum entropy change occurred at temperatures associated with T_c and is negative for all samples (- ΔS_m). Graphs of -ΔS_m *vs* T in $\mu_0 \Delta H$ = 1 T, 2 T, 3 T and 4 T reveal higher absolute value $|\Delta S_M|$ for polycrystalline samples with a generally narrower bell shaped curve around T_c. The values for maximum entropy change and are equal or higher than those for other polycrystalline compounds undergoing only second order transition, studied in this work or reported in literature. Values of entropy change are presented in the Table 6.3.

6.2.9 Magnetic entropy change in nano-scale $Pr_{0.65-x}Nd_xSr_{0.35}MnO_3$ compounds

All samples exhibit negative entropy change with maximum $|\Delta S_M|$ occurring at temperatures close to T_c. The bell-shaped curve is most noticeable in the graph for x = 0.05 sample. The curve widens with subsequent substitution, with curves below the peak resembling a straight line with some fluctuations for samples x = 0.25 and x = 0.35. These features have been attributed to mixed magnetic phases in other studies [158], but most likely this behavior suggests higher anisotropy for samples with higher Nd^{3+} content. Additionally, the curves become sharper with higher external fields, as more particles come under the influence of the field. This is in contrast to the bulk compounds where the bell-shaped curve tends to widen with higher fields.

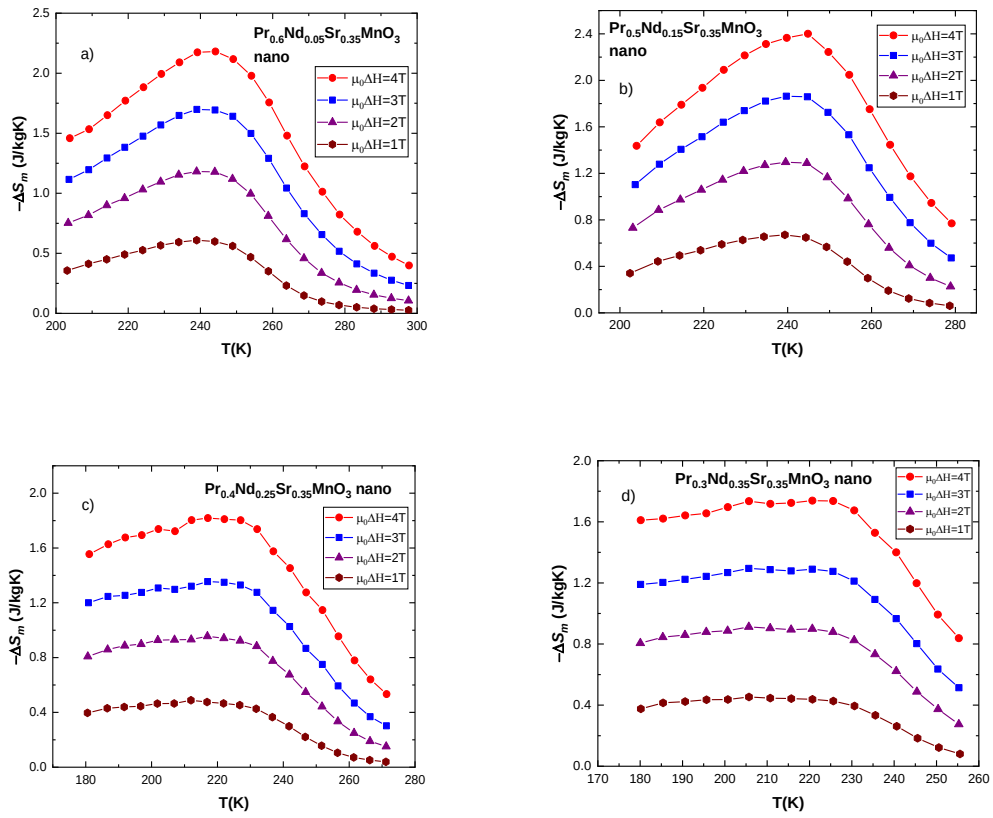

Figure 6.7 Magnetic entropy change vs temperature (-ΔS_M vs T) graphs for nano-scale $Pr_{0.65-x}Nd_xSr_{0.35}MnO_3$ samples. a) x=0.05 b) x=0.15 c) x=0.25 d) x=0.35 [191].

6.2.10 Magnetocaloric effect in polycrystalline and nano-scale $Pr_{0.65-x}Nd_xSr_{0.35}MnO_3$ compounds

For the purpose of estimating material's true cooling potential, we have calculated a couple of figures-of-merit, namely Relative cooling power (*RCP*) and Time-averaged entropy change (*TEC*). All samples exhibit fairly large values of *RCP* comparable to other investigated systems. Values are presented in the Figure 6.3.

Table 6.3 Experimental values for $Pr_{0.65-x}Nd_xSr_{0.35}MnO_3$ materials: magnetic measurements [191].

Compound	T_C (K)	M_s (μ_B/f.u.)	M_r (μ_B/f.u.)	M_r/M_s	H_{ci} (Oe)	$\lvert\Delta S_M\rvert$ (J/kgK) $\mu_0\Delta H$ = 1 T	$\lvert\Delta S_M\rvert$ (J/kgK) $\mu_0\Delta H$ = 4 T	RCP (*S*) (J/kg) $\mu_0\Delta H$ = 1 T	RCP (*S*) (J/kg) $\mu_0\Delta H$ = 4 T
$Pr_{0.65}Sr_{0.35}MnO_3$ (bulk)[74]	295					2.3			
$Pr_{0.6}Nd_{0.05}Sr_{0.35}MnO_3$	284	3.83	0.24	0.06	190	1.97	4.87	35	170
$Pr_{0.5}Nd_{0.15}Sr_{0.35}MnO_3$	279	4.1	0.3	0.07	180	2.17	5.36	39	193
$Pr_{0.4}Nd_{0.25}Sr_{0.35}MnO_3$	271	4.17	0.49	0.12	210	2.17	5.74	43	189
$Pr_{0.3}Nd_{0.35}Sr_{0.35}MnO_3$	268	-			-	1.48	4.39	44	197
$Pr_{0.65}Sr_{0.35}MnO_3$ (nano)	255	2.95	1.14	0.39	810	0.54	2.05	24	102
$Pr_{0.6}Nd_{0.05}Sr_{0.35}MnO_3$	251	3.07	1.15	0.37	870	0.61	2.18	37	174
$Pr_{0.5}Nd_{0.15}Sr_{0.35}MnO_3$	246	2.96	1.19	0.4	960	0.67	2.4	37	168
$Pr_{0.4}Nd_{0.25}Sr_{0.35}MnO_3$	229	2.94	1.13	0.38	860	0.49	1.82	39	164
$Pr_{0.3}Nd_{0.35}Sr_{0.35}MnO_3$	224	2.97	1.11	0.37	830	0.45	1.74	36	174

In Figure 6.8 we present *TEC* values for polycrystalline and nano-scale compounds in $\Delta T_{H\text{-}C}$ = 5 – 50 K. Visual inspection of the plots reveals that bulk compounds show a sharper slope between $\Delta T_{H\text{-}C}$ = 5 K and $\Delta T_{H\text{-}C}$ = 50 K compared to nano-sized compounds. Additionally, the curve for nano-compounds show some local fluctuation – result of fluctuation in their entropy change curves.

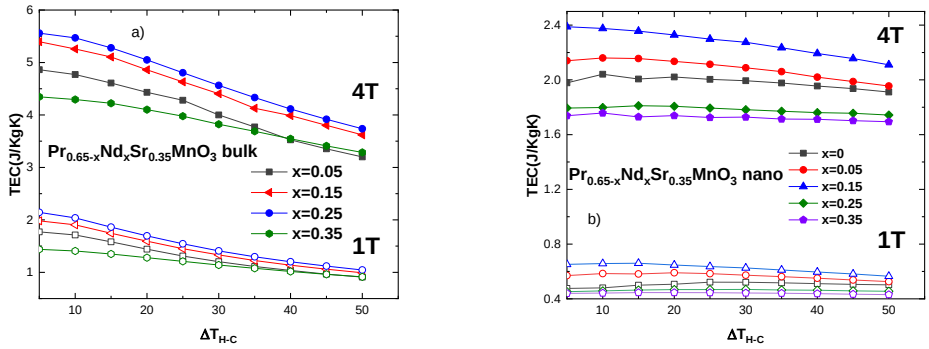

Figure 6.8 Temperature-averaged entropy change (TEC) vs $\Delta T_{H\text{-}C}$ for a) polycrystalline $Pr_{0.65-x}Nd_xSr_{0.35}MnO_3$ b) nano-sized $Pr_{0.65-x}Nd_xSr_{0.35}MnO_3$ [191].

7. Conclusions

In this work, we had successfully prepared and investigated a series of polycrystalline and nanocrystalline perovskite manganites.

We had prepared $La_{0.7-x}Eu_xBa_{0.3}MnO_3$, $La_{0.7-x}Ho_xBa_{0.3}MnO_3$, and $La_{0.7}Ba_{0.3-x}Ca_xMnO_3$ based on the knowledge that the parent bulk compound $La_{0.7}Ba_{0.3}MnO_3$ shows *CMR* properties and excellent magnetocaloric values at Curie temperature of around 340 K. Inclusion of smaller ions at the A-site brought the T_c values lower to the near room temperature values, with high values of entropy change. In addition, we prepared and investigated nano-scale compounds for each of the aforementioned compounds for their novel physical properties and flexibility in use.

We had also prepared and investigated $Pr_{0.65}Sr_{0.35-x}Ca_xMnO_3$ and $Pr_{0.65-x}Nd_xSr_{0.35}MnO_3$ polycrystalline and nanocrystalline compounds on the similar idea that the parent bulk compound $Pr_{0.65}Sr_{0.35}MnO_3$ possesses interesting electrical and magnetic properties as well as near room temperature T_c = 295 K. Inclusion of narrow banded Ca^{2+} and Nd^{3+} ions brought on some interesting results such as change in structure and in electrical and magnetic properties. Lower values of T_c with possibility of finer control were achieved. Large values of entropy change, particularly for the samples with first order transitions were observed.

Bibliography

[1] H.W. Meyer, *A history of electricity and magnetism*. Burndy library. 1972.

[2] J.M.D. Coey, M. Viret, S. Von Molnár, *Mixed-Valence Manganites*. Adv. Phys., *48*, 167–293. 1999, https://doi.org/10.1080/000187399243455.

[3] K. Uchida, J. Xiao, H. Adachi, J, Ohe, S. Takahashi, J. Ieda, T. Ota, Y, Kajiwara, H. Umezawa, H. Kawai, G. E. W. Bauer, S. Maekawa, E. Saitoh, *Spin Seebeck Insulator*, Nature Matter. 9, 894, 2010.

[4] V.E. Salazar-Munoz; A. Lobo Guerrero; S.A. Palomares-Sanchez, Review of magnetocaloric properties in lanthanum manganites. *J. Magn. Magn. Mater* 562, 2022, https://doi.org/10.1016/j.jmmm.2022.169787.

[5] E. Dagotto, T. Hotta, A. Moreo, Colossal Magnetoresistant Materials: The Key Role of Phase Separation, *Phys. Rep.* 344, 1-3, 1–153. 2001.

[6] K.A. Gschneidner, V.K. Pecharsky, Thirty Years of near Room Temperature Magnetic Cooling: Where We Are Today and Future Prospects. *Int. J. Refrig.* 31, 945–961, 2008, https://doi.org/10.1016/j.ijrefrig.2008.01.004.

[7] P. Ramirez, Colossal Magnetoresistance. *Journal of Physics: condensed matter*. 9(39), 1999, DOI: 10.1088/0953-8984/9/39/005.

[8] E. Pavarini, E. Koch, F. Anders, M. Jarrell, *Correlated Electrons: From Models to Materials Modeling and Simulation*; Forschungszentrum Julich: Jülich, Germany; Chapter 7, Volume 2, pp. 18–21, ISBN 978-3-89336-796-2. 2012.

[9] C. N. R. Rao, *Perovskites.* In *Encyclopedia of Physical Science and Technology*; Elsevier, pp. 707–714. 2003.
[10] Y. Tokura, Y. Tomioka, Colossal magnetoresistive manganites, *J. Magn. Magn. Mater*. 200, 1-3, 1-23,1999.
[11] K.G. Sandeman, Magnetocaloric materials: The search for new systems, *Scr. Mater., 67*, 566–571, 2012.
[12] K. Raju, S. P. Manjunathrao, Venugopal Reddy, Correlation between Charge, Spin and Lattice in La-Eu-Sr Manganites. *J. Low Temp. Phys.*, *168*, 334–349. 2012, https://doi.org/10.1007/s10909-012-0630-7.
[13] C. Krishnamoorthi, S.K. Barik, Z. Siu, R. Mahendiran, Normal and inverse magnetocaloric effects in $La_{0.5}Ca_{0.5}Mn_{1-x}Ni_xO_3$. *Solid State Commun*., *150*, 1670–1673, 2010.
[14] M.H. Phan, T.L. Phan, S.C. Yu, N.D. Tho, N, Chau, Large magnetocaloric effect in $La_{0.845}Sr0_{.155}Mn_{1-x}MxO_3$ (M = Mn, Cu, Co) perovskites, *Phys. Stat. Sol. (b)* 241, 1744, 2004.
[15] I. Montoya De Los Santos, Hugo J. Cortina-Marrero, M.A. Ruíz-Sánchez, L. Hechavarría-Difur, F.J. Sánchez-Rodríguez, Maykel Courel, Hailin Hu, Optimization of $CH_3NH_3PbI_3$ perovskite solar cells: A theoretical and experimental study, *Solar Energy*, 199, 198-205, 2020, ISSN 0038-092X, https://doi.org/10.1016/j.solener.2020.02.026.
[16] D.V. Maheswar Repaka, Magnetic control of spin entropy, thermoelectricity and electrical resistivity in selected manganites, Phd thesis, *M.Tech. Indian Institute of technology*, Kharagpur, India, 2014.
[17] J. Kanamori, Crystal distortion in magnetic compounds, *J. Appl. Phys*. 31, 14S, 1960.
[18] E. Dagotto, *Nanoscale Phase Separation and Colossal Magnetoresistance*, 1st ed.; Springer Science & Business Media: New York, NY, USA, pp. 271–284. 2002.
[19] Y.A. Isyumov, Y, N. Skryabin, Double exchange model and the unique properties of the manganites, *Phys.-Usp.* 44 109, 2001.
[20] P.W. Anderson, New approach to the theory of superexchange Interractions, *Phys. Rev*. 115, 2, 1959.
[21] T. Dietl, Exchange interactions: super-exchange, double exchange, RKKY; magnetic orders, *Analele Universităţii de Vest din Timişoara* Vol. LIII, Seria Fizică, 2009.
[22] E. Koch, *Exchange Mechanisms* Computational Materials Science. German Research School for Simulation Sciences, 1977.
[23] Pawel Gruszecki, at al, *The influence of the internal domain wall structure on spin wave band structure in periodic magnetic stripe domain patterns, chapter two*, Solid State Physics 72, 29-82, 2021.
[24] J. Kanamori, Superexchange interactions and symmetry properties of electron orbitals, *J.Phys. Chem. Solid* 10, 87, 1959.
[25] J.B. Goodenough, Theory of the role of covalence in the perovskite-type Manganites, *Phys. Rev*. 100, 564, 1955.
[26] C. Zener, Interactions between d shells in the transition metals, *Phys. Rev*. 81, 440, 1951
[27] A.M. Tishin Y.I. Spichkin, *The magnetocaloric effect and its applications*, CRC press, Boca Raton, 2003.
[28] J.W. Verwey, Electronic Conduction of Magnetite (Fe_3O_4) and its Transition Point at Low Temperatures, *Nature*, 144, 327, 1939.

[29] C.H. Chen, S. W. Cheong, Commensurate to Incommensurate Charge Ordering and Its Real-Space Images in La0.5Ca0.5MnO3, *Phys. Rev. Lett*. 76, 4042, 1996.
[30] I.G. Deac, R. Tetean, E. Burzo, Phase Separation, Transport and Magnetic Properties of $La_{2/3}A_{1/3}Mn_{1-X}Co_xO_3$, A = Ca, Sr ($0.5 \leq x \leq 1$). *Phys. B Condens. Matter 403*, 1622–1624. 2008 , https://doi.org/10.1016/j.physb.2007.10.203.
[31] C.N.R. Rao, Charge, Spin, and Orbital Ordering in the Perovskite Manganates, $Ln_{1-x}A_xMnO_3$ (Ln = Rare Earth, A = Ca or Sr). *J. Phys. Chem. B, 104,* 5877–5889. 2000 https://doi.org/10.1021/jp0004866.
[32] K. Ebata at al, Chemical potential shift induced by double-exchange and polaronic effects in $Nd_{1-x}Sr_xMnO_3$, *Phys. Rev. B* 77(9), 2008.
[33] A. Sakka at al, Impact of synthesis routes on normal and inverse magnetocaloric effects and critical behaviour in the charge-ordered $Pr_{0.5}Sr_{0.5}MnO_3$ manganite, *The European Physical Journal plus,* 134(5), 2019.
[34] Badea C., Tetean R., Deac I.G. Suppression of Charge and Antiferromagnetic Ordering in Ga-doped $La_{0.4}Ca_{0.6}MnO_3$, *Rom. J. Phys.*, 63, 604, 2018.
[35] M. Coey, Charge ordering in oxides, *Nature*, 430, 155, 2004.
[36] P. Schiffer, A.P. Ramirez, W. Bao, S-W. Cheong, Low Temperature Magnetoresistance and the Magnetic Phase Diagram of La1−*x*Ca*x*MnO3, *Phys. Rev. Lett*. 75, 3336, 1995.
[37] R. Mohan, at al, Colossal electroresistance in Sm0.55Sr0.45MnO3, *J. Alloys Compnd* 508, L32-L35, 2010.
[38] N. Ibrahim, N. A. M. Rusop,R. Rozilah,N. Asmira,A.K. Yahya, Effect of grain modification on electrical transport properties and electroresistance behavior of $Sm_{0.55}Sr_{0.45}MnO_3$. *Int. J. Eng. Technol. 7*, 113–117, 2018.
[39] A.J. Millis, P.B. Littlewood, B.I. Shraiman, double exchange alone does not explain the the resistivity in $La_{1-x}Sr_xMnO_3$, Phys. Rev. Lett. 74, 5144, 1995.
[40] K. Kubo, N. Ohata, N. A Quantum Theory of Double Exchange. *J. Phys. Soc. Jpn*. *33*, 21–32. 1972.
[41] H. E. Stanley, Scaling, universality, and renormalization: three pillars of modern critical phenomena, *Rev. Mod. Phys.* 71, 1999.
[42] H.E. Stanley, *Introduction to Phase Transitions and Critical Phenomena*; Oxford University Press: Oxford, UK, pp. 7–10, 1987.
[43] M.M. Ansanelli, Critical exponents and the renormalization group, 2019, *unpublished.*
[44] A. Varvescu, I.G. Deac, Critical Magnetic Behavior and Large Magnetocaloric Effect in $Pr_{0.67}Ba_{0.33}MnO_3$ Perovskite Manganite. *Phys. B Condens. Matter*, *470–471*, 96–101. 2015 https://doi.org/10.1016/j.physb.2015.04.037.
[45] M. Jeddi, H. Gharsallah, M. Bejar, M. Bekri,E. Dhahri, E. K. Hlil, Magnetocaloric Study, Critical Behavior and Spontaneous Magnetization Estimation in $La_{0.6}Ca_{0.3}Sr_{0.1}MnO_3$ Perovskite, *RSC Adv. 8*, 9430–9439. 2018, https://doi.org/10.1039/c8ra00001h.
[46] A. Arrott, Criterion for Ferromagnetism from Observations of Magnetic Isotherms. *Phys. Rev*. 108, 1394–1396., 1957.
[47] A. Arrott, J.E. Noakes, Approximate Equation of State for Nickel Near Its Critical Temperature. *Phys. Rev. Lett. 19*, 786–789., 1967.

[48] P. Simidzija, Critical Phenomena and the renormalization group, *University of British Columbia*, 2019, *unpublished.*

[49] B.K. Banerjee, On a Generalised Approach to First and Second Order Magnetic Transitions. *Phys. Lett. 12*, 16–17., 1964 https://doi.org/10.1016/0031-9163(64)91158-8.

[50] J.S. Kouvel, M.E. Fisher, Detailed magnetic behavior of nickel near its Curie point, *Phys. Rev.* 136, A1626, 1964.

[51] S. Vadnala, S. Asthana, Magnetocaloric effect and critical field analysis in Eu substituted $La_{0.7-x}Eu_xSr_{0.3}MnO_3$ (x=0.0, 0.1, 0.2, 0.3) manganites. *J. Magn. Magn. Mater.*, *446*, 68–79, 2018, ISSN 0304-8853. https://doi.org/10.1016/j.jmmm.2017.09.001.

[51] M. E. Fisher, S.K. Ma, B.G. Nickel, Critical Exponents for Long-Range Interactions. *Phys. Rev. Lett.*, *29*, 917. 1972.

[52] R.K. Pathria, P.D. Beale, *Phase Transitions: Criticality, Universality, and Scaling*. In *Statistical Mechanics*; Elsevier: Amsterdam, The Netherlands, pp. 417–486. 2022.

[53] D. Kim, at al, Tricritical Point and the Doping Dependence of the Order of the Ferromagnetic Phase Transition of $La_{1\_x}Ca_xMnO_3$, *Phys. Rev. Lett*. 89, 22, 2002.

[54] H.S. Shin, at al, First-order-like transitions in manganite oxide $La_{0.7}Ca_{0.3}MnO_3$, *Solid state commun.*, 118, 377-380, 2001.

[55] M.H. Phan, at al, Tricritical point and critical exponents of $La_{0.7}Ca_{1-x}Sr_xMnO_3$, *J. Alloys Compnd*., 508, 238-244, 2010.

[56] K. Dhahri, at al, Critical phenomena and estimation of the spontaneous magnetization from a mean field analysis of the magnetic entropy change in $La_{0.7}Ca_{0.1}Pb_{0.2}Mn_{0.95}Al_{0.025}Sn_{0.025}O_3$, *RSC adv*. 8, 3099, 2018.

[57] A. Smith, Who discovered the magnetocaloric effect?, Warburg, Weiss, and the connection between magnetism and heat, *Eur. Phys. J. H* 38, 507-517, 2013.

[58] W.F. Giauque, I.P.D. Mcdougall, Attainment of temperatures below 1° absolute by demagnetization of $Gd_2(SO_4)_3{\cdot}8H_2O$, *Phys. Rev*. 43, 768, 1933.

[59] V. K. Pecharsky and K. A. Gschneidner, Jr., Giant Magnetocaloric Effect in Gd5(Si2Ge2), *Phys. Rev. Lett.* 78, 4494, 1997.

[60] P. J. von Ranke at al, Calculation of the giant magnetocaloric effect in the MnFeP0.45 As0.55 compound, *Phys. Rev B cond. matt.* 70, 2004.

[61] E. Bruck, Development of magnetocaloric refrigeration, *J. Phys. D: Appl. Phys.* 38, R381, 2005.

[62] B.G. Shen, at al, Recent Progress in Exploring Magnetocaloric Materials, *Adv. Mat*. 21, 4545, 2009.

[63] D.T. Cam Thanh, at al, Magnetocaloric effect in MnFe(P,Si,Ge) compounds, *J. Appl. Phys*. 99, 08Q107, 2006.

[64] F.X. Hu, B.G. Shen, J, R. Sun, G.H. Wu, Large magnetic entropy change in a Heusler alloy Ni52.6Mn23.1Ga24.3 single crystal, *Phys. Rev. B* 64, 132412, 2001.

[65] B. Brindle, "Magnetic Air Conditioners: A High Tech Way Of Keeping Cool" 29 August 2012.HowStuffWorks.com.<https://home.howstuffworks.com/magnetic-air-conditioner.htm> , 22 May, 2024.

[66] K.P. Lim, S.W. Ng, S.A. Halim, S.K. Chen and J.K. Wong Effect of Divalent Ions (A = Ca, Ba and Sr) Substitution in La-A-Mn-O Manganite on Structural, Magnetic and Electrical Transport Properties, *Am. J. Appl. Sci.* 6 (6): 1153-1157, 2009.

[67] W. Cui, W. Liu, Z. Zhang, The origin of large overestimation of the magnetic entropy changes calculated directly by Maxwell relation, *Appl. Phys. Lett*. 96, 222509, 2010.
[68] V.K. Pecharski, K.A. Gschneidner Jr, *Magnetocaloric effect, Encyclopedia of condensed matter physics*, Elsevier, pp. 236-244, 2005.
[69] I.G. Deac, A. Vladescu, Magnetic and magnetocaloric properties of Pr1−xSrxCoO3 cobaltites, *J. Magn. Magn. Mater.* 365, 1–7. 2014.
[70] V. Zverev, A.M. Tishin, *Magnetocaloric Effect: From Theory to Practice. In Reference Module in Materials Science and Material Engineering*; Elsevier: Amsterdam, The Netherlands, 5035–5041. 2016 https://doi.org/10.1016/B978-0-12-803581-8.02813-7.
[71] L.D. Griffith, Y. Mudryk, J. Slaughter, V.K. Pecharsky, Material-based figure of merit for caloric materials, *J. Appl. Phys*., 123, 034902, 2018.
[72] A. Smith, A.C.R.H. Bahl, R. Bjørk, K. Engelbrecht, K. Kaspar, K.K. Nielsen, N. Pryds, Materials challenges for high performance magnetocaloric refrigeration devices, *Adv. Energy Mater* 2, 1288–1318, 2012.
[73] A. Kitanovski, J. Tusek, U. Tomc, U. Plaznik, M. Ozbolt, A. Poredos, *Magnetocaloric Energy Conversion: From Theory to Applications,* 1st ed.; Springer: New York, NY, USA, 2015. https://doi.org/10.1007/978-3-319-08741-2_10.
[74] F. Guillou, U. Legait, A. Kedous-Lebouc, V. Hardy, Development of a new magnetocaloric material used in a magnetic refrigeration device. *EPJ Web Conf., 29*, 21, 2012, https://doi.org/10.1051/epjconf/20122900021.
[75] U. Legait, F. Guillou, A. Kedous-Lebouc, A.V. Hardy, M. Almanza, An experimental comparison of four magnetocaloric regenerators using three different materials. *Int. J. Refrig*. *37*, 147–155, 2014.
[76] P.J. von Ranke, at al, Understanding the inverse magnetocaloric effect in antiferro- and ferromagnetic arrangements, *J. Phys.: Cond. Matt*. 21, 056004, 2009.
[77] N.H. Duc, at al, Magnetic Properties and Magnetocaloric Effect in $Ni_{0.5}Mn_{0.5-x}Sb_x$ *Alloys, J. Korean Phys. Scociety* 60, 2012.
[78] R. J. Joenk, Adiabatic magnetization of antiferromagnets, *J. Appl. Phys*. 34, 1097, 1963.
[79] X. Moya, at al, Cooling and heating by adiabatic magnetization in the Ni50Mn34In16 magnetic shape-memory alloys, *Phys. Rev. B* 75, 184412, 2007.
[80] F. Casanova, A. Labarta, X. Batlle, F. J. Perez-Reche, E. Vives, L. Manosa, A. Planes, Direct observation of the magnetic-field-induced entropy change in Gd5(SixGe1−x)4 giant magnetocaloric alloys, *Appl. Phys. Lett*. 86, 262504, 2005.
[81] M. Quintero, J. Sacanell, L. Ghivelder, A. M. Gomes, A. G. Leyva, F. Parisi, *Appl. Phys. Lett*. 97, 121916, 2010.
[82] M. Quintero, at al, Magnetocaloric effect in phase separated manganites probed by differential thermal analysis, *Physisca B* 404, 2763, 2009.
[83] G. Souca, Magnetic Properties and Magnetocaloric Effect on Selected Rare Earth-Transition Metal Intermetallic Compounds. *Ph. D. Thesis, Babes-Bolyai University*, Cluj-Napoca, Romania, pp. 16-19, 2022, *unpublished.*
[84] S.Y. Dankov, A.M. Tishin, Magnetic phase transitions and the magnothermal properties of gadolinium, *Phys. Rev. B* 57, 3478, 1998.
[85] H. Huang, Z. B. Guo, D. H. Wang, Y. W. Du, Large magnetic entropy change in $La_{0.67-x}Gd_xCa_{0.33}MnO_3$, *J. Magn. Magn. Mater*. 173, 302, 1997.
[86] V.K. Pecharsky, K. A. Gschneidner Jr., *Adv. Cry. Eng.* 43, 1729, 1998.
[87] K. A. Gschneidner Jr., V.K. Pecharsky, A. O. Tsokol, Recent developments in magnetocaloric materials, *Rep. Prog. Phys.* 68, 1479, 2005.

[88] X. J. Niu, K.A. Gschneidner Jr., A. O. Pecharski, V.K. Pecharsky, Crystallography, magnetic properties and magnetocaloric effect in $Gd_4(Bi_xSb_{1-x})_3$ alloys. *J. Magn. Magn. Mater*. 234, 193, 2001.

[89] B. Kurniawan, S. Winarsih, C. Kurniawan, M. R. Ramadhan, and F. Ruli *Magnetic properties of polycrystalline $La_{0.7}Ba_{0.3}MnO_3$ for magnetocaloric effect application*. AIP Conference Proceedings 1862, 030061, 2017.

[90] W. Chen, L.Y. Nie, W. Zhong, Y.J. Shi, J.J. Hu, A.J. Li, Y.W. Du, Magnetocaloric effect in Nd doped perovskite $La_{0.7-x}Nd_xBa_{0.3}MnO_3$ polycrystalline near room temperature, *J. Alloys Compd.* 395, 23, 2005.

[91] N. Chau, at al, Sctructure, magnetic, magnetocaloric and magnetoresistance properties of $La_{1-x}Pb_xMnO_3$ perovskite, *Physica B Condens. Matter* 327, 270, 2003.

[92] S.G. Min, K.S. Kim, S.C. Yu, H. S. Suh, S.W. Lee, Magnetocaloric effect in $La_{1-x}Pb_xMnO_3$ (x = 0.1,0.2,0.3) compounds, *IEEE Trans. Magn*. 41, 2760, 2005.

[93] M.H. Phan, S.C. Yu, N.H. Hur, Excellent magnetocaloric properties of $La_{0.7}Ca_{0.3-x}Sr_xMnO_3$ single crystals, *Appl. Phys. Lett*. 86, 072504, 2005.

[94] M.H. Phan, T.L. Phan, S.C. Yu, N.D. Tho, N. Chau, Large magnetocaloric effect in $La_{0.845}Sr_{0.155}Mn_{1-x}MxO_3$ (M = Mn, Cu, Co) perovskites, *Phys. Stat. Sol. (b)* 241, 1744, 2004.

[95] A. Szewczyk, M. Gutowska, B. Dabrowski, T. Plackowski, N.P. Danilova, Y. P. Gaidukov, Specific heat anomalies in $La_{1-x}Sr_xMnO_3$, *Phys. Rev. B* 71, 224432, 2005.

[96] M.H. Phan, at al, Large magnetic entropy change above 300K in CMR materials, *J. Magn. Magn. Mater*. 258, 309, 2003.

[97] Z.B. Guo, Y.W. Du, J.S. Zhu, H. Huang, W.P. Ding, D. Feng, Large magnetic entropy change in perovskite type manganese oxides, *Phys. Rev. Lett*. 78, 1142, 1997.

[98] X. Bohigas, at al, Magnetic and calorimetric measurements on the magnetocaloric effect in $La_{0.6}Ca_{0.4}MnO_3$, *J. Magn. Magn. Mater.* 208, 85, 2000.

[99] A.K. Saw, G. Channagoudra, S. Hunagund, R.L. Hadimani, V. Dayal, Study of transport, magnetic and magnetocaloric properties in Sr^{2+} substituted praseodymium manganite. *Mater. Res. Express* 7, 016105, 2020 doi.org/10.1088/2053-1591/ab636d.

[100] M.H. Phan, S.C. Yu, Review of the magnetocaloric effect in manganite materials, *J.Magn. Magn. Mater.* 308, 325, 2007.

[101] N.T. Hien, N.P. Thuy, Preparation and magnetocaloric effect of $La_{1-x}Ag_xMnO_3$ (x = 0.1 – 0.3) perovskite compounds, *Physica B* 319, 168, 2002.

[102] N. Moutis, I. Panagiotopoulos, M. Pissas, D. Niarchos, Structural and magnetic properties of $La_{0.67}(Ba_xCa_{1-x})_{0.33}MnO_3$ perovskites (0<~x<~1). *Phys. Rev. B* 59, 2, 1999 doi: 10.1103/physrevb.59.1129.

[103] M. Pekala, V. Drozd, J.F. Fagnad, P. Vanderbemden, M. Ausloos, Magnetocaloric effect in nano- and polycrystalline $La_{0.7}Ca_{0.3}MnO_3$ manganites. *Applied physics A.* 90, 237-241, 2008.

[104] Badea, C.; Tetean, R.; Deac, I.G. Suppression of Charge and Antiferromagnetic Ordering in Ga-doped $La_{0.4}Ca_{0.6}MnO_3$. *Rom. J. Phys. 63*, 604. 2018.

[105] R.C. Bhatt, S.K. Singh, P.C. Srivastava, V.P.S. Agarwal, Awana, Impact of sintering temperature on room temperature magneto-resistive and magneto-caloric properties of Pr2/3Sr1/3MnO3. *J. alloys compd. 580, 377-381, 2013.*

[106] C.N.R. Rao, *Chemical Approaches to the synthesis of inorganic materials*, Whiley Eastern Ltd, New Delhi, 1994.

[107] D.D. Athayde, D.F. Souza, A.M.A. Silva, D. Vasconcelos, E.H.M. Nunes, D.d. Costa, W.L. Vasconcelos, Review of perovskite ceramic synthesis and membrane preparation methods. *Ceramics International* 42(6), 6555–6571, 2015.
[108] R. Vanelzuela, *Magnetic ceramics*, Cambridge university press, New York, 1994
[109] V. Pop, I. Chicinaș, and N. Jumate, *Fizica Materialelor: Metode Experimentale*. Presa Universitară Clujeană, 2001.
[110] R.A. Bortnic, at al., Synthesis of cobalt ferrite nanoparticles via a sol-gel combustion method, *Studia Universitatis Babes-Bolyai, Chemia*, 61, 4, 2016.
[111] R.A. Bortnic, at al, New Insights into the Magnetic Properties of $CoFe_2O_4$@SiO_2@Au Magnetoplasmonic Nanoparticles, *Nanomaterials* 12, 6, 2022.
[112] B. G. Rao, D. Mukherjee, B. M. Reddy, *Nanostruct. Novel Ther.*, 1–36, 2017.
[113] B.D. Cullity, *Elements of X-ray diffraction*, Addison-Wesley, Massachusetts, 1972.
[114] W.H. Bragg, W.L. Bragg, X Rays and Crystal Structure. *G. Bell and Sons, Ltd.* 1915.
[115] A.I. Smirnov, at al, Cryogen-free superconducting magnet system for multifrequency electron paramagnetic resonance up to 12.1 T, *Review of scientific instruments* 77, 035108 2006.
[116]Cryogenic, Ltd., VSM drawings, http://www.cryogenic.co.uk/sites/default/files/product_files/vsm_drawings.pdf, 2006.
[117] W.J. Wolfgong, Chemical Analysis Techniques for Failure Analysis. In *Handbook of Materials Failure Analysis with Case Studies from the Aerospace and Automotive Industries*, Butterworth-Heinemann, pp. 279-307. 2016.
[118] R. Tali, Determination of Average Oxidation State of Mn in $ScMnO_3$ and $CaMnO_3$ by Using Iodometric Titration. *Damascus Univ. J. Basic Sci. 23*, 9–19, 2007.
[119] F. Licci, G. Turilli, P. Ferro, Determination of Manganese Valence in Complex La-Mn Perovskites. *J. Magn. Magn. Mater. 164*, 1996, doi:10.1016/S0304-8853(96)00623-3.
[120] D. Arovas, Lecture notes on condensed matter physics (a work in progress), *CreateSpace Independent Publishing Platform*, 2014.
[121] M.H. Phan, S.B. Tian, S.C. Yu, A.N. Ulyanov, Magnetic and magnetocaloric properties of $La_{0.7}Ca_{0.3-x}Ba_xMnO_3$ compounds, *J. Magn and Magn. Mater*. 256, 1–3, 2003, 306-310, 2003.
[122] K.P. Lim, S.W. Ng, S.A. Halim, S.K. Chen and J.K. Wong Effect of Divalent Ions (A = Ca, Ba and Sr) Substitution in La-A-Mn-O Manganite on Structural, Magnetic and Electrical Transport Properties, *American Journal of Applied Sciences* 6 (6): 1153-1157, 2009.
[123] M. Pekala, V. Drozd, J.F. Fagnad, P. Vanderbemden, Magnetocaloric effect in nano- and polycrystalline $La_{0.5}Ca_{0.5}MnO_3$ manganites. *J. Alloys Compd.* 507, 350-355, 2010.
[124] D. Nath, F. Singh, R. Das, X-Ray Diffraction Analysis by Williamson-Hall, Halder-Wagner and Size-Strain Plot Methods of CdSe Nanoparticles- a Comparative Study. *Mater. Chem. Phys.***,** *239*, 2020, doi:10.1016/j.matchemphys.2019.122021.
[125] M.B. Salamon, M. Jaime, The physics of manganites: Structure and transport, *Rev. Mod. Phys*. 73, 583, 2001.
[126] S. V. Trukhanov, A.V. Trukhanov, S.G. Stepin, H. Szymczak, and C.E. Botez, Effect of the size factor on the magnetic properties of manganite $La_{0.50}Ba_{0.50}MnO_3$. *Phys. Solid State* 50, 5, 2008, doi: 10.1134/S1063783408050144.

[127] D.D. Majumder, D.D. Majumder, Karan S. Magnetic Properties of Ceramic Nanocomposites. *Ceramic Nanocomposites*, Composites Science and Engineering, Elsevier B.V.: Amsterdam, The Netherlands, 51–91. 2013.

[128] N.A. Liedienov, Z. Wei, V.M. Kalita, A.V. Pashchenko, Q. Li, I.V. Fesych, V.A. Turchenko, C.X. Wei, B. Liu, A.T. Kozakov, G.G. Levchenko, Spin-dependent magnetism and superparamagnetic contribution to the magnetocaloric effect of non-stoichiometric manganite nanoparticles. *Appl. Mater. Today. 26*, 101340, 2022.

[129] D. Nath, F. Singh, R. Das, X-Ray Diffraction Analysis by Williamson-Hall, Halder-Wagner and Size-Strain Plot Methods of CdSe Nanoparticles- a Comparative Study. *Mater. Chem. Phys. 239*, 2020, doi:10.1016/j.matchemphys.2019.122021.

[130] R.D. Shannon, Revised effective ionic radii and systematic studies of interatomic distances in halides and chalcogenides. *Acta Crystallogr*., A 32, 751. 1976.

[131] R. Atanasov, Physical properties and magnetocaloric effect at roon temperature of $La_{0.7-x}Eu_xBa_{0.3}MnO_3$ compounds, Ms. Thesis, Babes-Bolyai University, Cluj-Napoca, Romania, 2018, *unpublished*.

[132] R. Atanasov, R. Bortnic, R. Hirian, E. Covaci, T. Frentiu, F. Popa, and I. G. Deac, Magnetic and Magnetocaloric Properties of Nano- and Polycrystalline Manganites La(0.7−x)EuxBa0.3MnO3, *Materials*, *15*(21), 7645, 2022.

[133] R. Gross, L. Alff, B. Büchner, B.H. Freitag, C. Höfener, J. Klein, Y. Lu, W. Mader, J.B. Philipp, M.S.R. Rao, et al. Physics of Grain Boundaries in the Colossal Magnetoresistance Manganites. *J. Magn. Magn. Mater. 211*, 2000, doi:10.1016/S0304-8853(99)00727-1.

[134] N. Panwar, D.K. Pandya, S.K. Agarwal, Magneto-Transport and Magnetization Studies of $Pr_{2/3}Ba_{1/3}MnO_3$:Ag_2O composite manganites. *J. Phys.: Condens. Matter* 19, 456224, 2007.

[135] N. Panwar, D.K. Pandya, A. Rao, K.K. Wu, N. Kaurav, Y.K. Kuo, S.K. Agarwal, Electrical and Thermal Properties of $Pr_{2/3}(Ba_{1-X}Cs_x)_{1/3}MnO_3$ Manganites. *Eur. Phys. J. B*, *65*, 2008, doi:10.1140/epjb/e2008-00331-6.

[136] P.A. Joy, P.S. Anil Kumar, S.K. Date, The Relationship between Field-Cooled and Zero-Field-Cooled Susceptibilities of Some Ordered Magnetic Systems. *J. Phys. Condens. Matter* 10, 1998, doi:10.1088/0953-8984/10/48/024.

[137] R. Pelka, P. Konieczny, M. Fitta, M. Czapla, P.M. Zielinski, M. Balanda, T. Wasiutynski, Y. Miyazaki, A. Inaba, D. Pinkowicz, et al., Magnetic systems at criticality: Different signatures of scaling. *Acta Phys. Pol. 124*, 977, 2013.

[138] N.A. Liedienov**,** A.V. Pashchenko**,** V.P. Pashchenko**,** V.K. Prokopenko**,** Revenko, Yu. F**.** Structure defects, phase transitions, magnetic resonance and magneto-transport properties of $La_{0.6-x}Eu_xSr_{0.3}Mn_{1.1}O_{3-\delta}$ceramics.*LowTemp.Phys.*,42,1102,2016, doi.org/10.1063/1.4973538.

[139] B. Arun, M.V. Suneesh, M. Vasundhara, Comparative Study of Magnetic Ordering and Electrical Transport in Bulk and Nano- Grained $Nd_{0.67}Sr_{0.33}MnO_3$ Manganites. *J. Magn. Magn. Mater. 418*, 2016, doi:10.1016/j.jmmm.2016.01.096.

[140] J.A. Peters, Relaxivity of Manganese Ferrite Nanoparticles. *Prog. Nucl. Magn. Reson. Spectrosc., 120–121*, 2020.

[141] M. Ziese, Critical scaling and percolation in manganite films, *J. Phys.: Condens. Matter* 13, 2919, 2001.

[142] M. Smari, I. Walha, A. Omri, A; J.J. Rousseau, E. Dhari, E.K. Hlil, Critical parameters near the ferromagnetic–paramagnetic phase transition in $La_{0.5}Ca_{0.5-x}Ag_xMnO_3$ compounds ($0.1 \leq x \leq 0.2$). *Ceram. Int.* 40, 8945-8951, 2014.

[143] D. Shi, M. Ye, L. Zhao, at al, Critical properties of perovskite manganite $La_{0.88}Sr_{0.12}MnO_3$ nanocrystalline, *J. Sol-gel sci. tech.* 107, 3, 1-8, 2023.

[144] A. Gómez, J.L. Izquierdo, I. Supelano, C.A. Parra, E. Chavarriaga, O. Morán, Ferromagnetic long-range ordering in nano-crystalline $La_{0.7}Ca_{0.3}Mn_{1-x}Ni_xO_3$ ($x = 0, 0.02$) manganites, *J. Magn. Magn. Mater.*, 475, 524-532, 2019, ISSN 0304-8853.

[145] A. Tozri, Sh. Alhalafi, Ziyad A. Alrowaili, Mongi Horchani, Aref Omri, R. Skini, S. Ghorai, A. Benali, Benilde F.O. Costa, Gulce O. Ildiz, Investigation of the magnetocaloric effect and the critical behavior of the interacting superparamagnetic nanoparticles of $La_{0.8}Sr_{0.15}Na_{0.05}MnO_3$, *J. Alloys Compd.*, 890, 161739, 2022, ISSN 0925-8388,

[146] D. Turki, Z.K. Ghouri, S. Al-Meer, K. Elsaid, M.I. Ahmad, A. Easa, G. Remenyi, S. Mahmood, E.K. Hlil, M. Ellouze, et al. Critical Behavior of $La_{0.8}Ca_{0.2}Mn_{1-x}Co_xO_3$ Perovskite ($0.1 \leq x \leq 0.3$). *Magnetochemistry 3*, 28., 2017.

[147] V. Pecharsky, A. Holm, K. Gschneidner Jr, and R. Rink, Massive magnetic-field-induced structural transformation in Gd5Ge4 and the nature of the giant magnetocaloric effect, *Phys. Rev. Lett*. 91, 197204, 2003.

[148] M. Kuz'Min, Factors limiting the operation frequency of magnetic refrigerators, *Appl. Phys, Lett*. 90, 251916, 2007.

[149] L. Patra, B. Liao, Indirect Exchange Interaction Leads to Large Lattice Contribution to Magnetocaloric Entropy Change, *Phys. Rev. Lett*. 131, 066703, 2023.

[150] M.A. Hamad, Magnetocaloric effect in $La_{0.65-x}Eu_xSr_{0.35}MnO_3$. *Phase Transitions*, 87(5), 460–467, 2014.

[151] Zhiwei Gong, Wei Xu; N. A. Liedienov, D.S. Butenko, I.V. Zatovsky, I.A. Gural'skiy, Ziyu Wei,; Quanjun Li,; Bingbing Liu,; Yu A Batman,; A.V. Pashchenko , G.G. Levchenko, Expansion of the multifunctionality in off-stoichiometric manganites using post-annealing and high pressure: physical and electrochemical studies. *Phys Chem. Chem. Phys*. 24(36), 21872-21885, 2002, doi: 10.1039/d2cp01959k.

[152] W. Archibald, J.S. Zhou, J. Goodenough, First order transition at T_c in the orthomanganites, *Phys. Rev.* B 53, 14445, 1996.

[153] M. Pekala, V. Drozd, Magnetocaloric effect in nano- and polycrystalline $La_{0.8}Sr_{0.2}MnO_3$ manganites. *J. alloys compd*. 456, 30-33., 2008.

[154] V.B. Naik, S.K. Barik, R. Mahendiran, B. Raveau, Magnetic and Calorimetric Investigations of Inverse Magnetocaloric Effect in $Pr_{0.46}$ $Sr_{0.54}$ MnO_3. *Appl. Phys. Lett.*, *98*, 2011, doi:10.1063/1.3567760.

[155] M.H. Ehsani, P. Kameli, M.E. Ghazi, F.S. Razavi, M. Taheri, Tunable magnetic and magnetocaloric properties of $La_{0.6}Sr_{0.4}MnO_3$ nanoparticles. *J. Appl. Phys.*, 114, 223907, 2013, doi.org/10.1063/1.4846758.

[156] L.E. Hueso, P. Sande, D.R. Miguéns, J. Rivas, F. Rivadulla, M.A. López-Quintela, Tuning of the magnetocaloric effect in nanoparticles synthesized by sol–gel techniques. *J. Appl. Phys*. *91*, 9943–9947. 2002, https://doi.org/10.1063/1.1476972.

[157] J.S. Amaral, M.S. Reis, V.S. Amaral, T.M. Mendonca, J.P. Araujo, M.A. Sa, P.B. Tavares, J.M. Vieira, Magnetocaloric effect in Er- and Eu-substituted ferromagneticLa-Sr manganites. *J. Magn. Magn. Mater.* 290, 686-689., 2009.

[158] B. Anis, S. Tapas, S. Banerjee, I. Das, Magnetocaloric properties of nanocrystalline $Pr_{0.65}(Ca_{0.6}Sr_{0.4})_{0.35}MnO_{3..}$ *J. Appl. Phys*. 103, 013912, 2008 doi: 10.1063/1.2832431.

[159] C.L. Wang, J. Liu, Y. Mudryk, Y.J. Zhu, Y. Fu Bin Long, V.K. Pecharsky, Magnetic and magnetocaloric properties of $DyCo_2C_x$ alloys. *J. Alloys Compd. 777*, 152–156., 2019 https://doi.org/10.1016/j.jallcom.2018.10.169.

[160] D. Mazumdar, K. Das, I. Das, Study of magnetocaloric effect and critical exponents in polycrystalline $La_{0.4}Pr_{0.3}Ba_{0.3}MnO_3$ compounds. *J. Appl. Phys*. *127*, 093902, 2020.

[161] B. Lorentz, A. P. Litvinchuk, M. M. Gospodinov, C. W. Chu, Field-Induced Reentrant Novel Phase and a Ferroelectric-Magnetic Order Coupling in HoMnO3, *Phys. Rev. Lett*. 92, 087204, 2004.

[162] A. Muñoz, J. A. Alonso, M. J. Martínez-Lope, M. T. Casáis, J. L. Martínez, M. T. Fernández-Díaz, Evolution of the Magnetic Structure of Hexagonal $HoMnO_3$ from Neutron Powder Diffraction Data, *Chem. Mater*. 13, 5, 1497–1505, 2001.

[163] W Boujelben, A Cheikh-Rouhou, J. Pierre, J.C Joubert, Effect of quenching on magnetic properties of polycrystalline $Pr_{0.5}Sr_{0.5}MnO_3$ perovskite manganite, *J. Alloys Compd.* 314, 1–2, 15-21, 2001.

[164] L.E. Hueso, J. Rivas, F. Rivadulla, M.A. López-Quintela, Tuning of Colossal Magnetoresistance via Grain Size Change in $La_{0.67}Ca_{0.33}MnO_3$, *J. Appl. Phys*. 86(7), 3881-3884, 1999.

[165] V. Podzorov, B. G. Kim, V. Kiryukhin, M. E. Gershenson, S-W. Cheong, Martensitic accommodation strain and the metal-insulator transition in manganites, *Phys. Rev. B* 64, 140406(R), 2001.

[166] P. Raychaudhuri, at al, The effect of holmium doping on the magnetic and transport properties of $La_{0.7-x}Ho_xSr_{0.3}MnO_3$ ($0 \leq x \leq 0.4$), *J. Condens. Matter phys.* 9(49):10919, 1999.

[167] A. Rostamnejadi, M. Venkatesan, J. Alaria, M. Boese, P. Kameli, H. Salamati, J.M.D. Coey, Conventional and Inverse Magnetocaloric Effects in $La_{0.45}Sr_{0.55}MnO_3$ Nanoparticles. *J. Appl. Phys.* 110, 043905., 2011 https://doi.org/10.1063/1.3614586.

[168] V. Franco, J.S. Blázquez, B. Ingale, A. Conde, The Magnetocaloric Effect and Magnetic Refrigeration Near Room Temperature: Materials and Models, *Annu. Rev. Mater. Res*. 42, 2012.

[169] A. Espinosa, M. Otero-Leal, F. Rivadulla, J. Rivas, A. de Andrés, Electron-phonon coupling through the orthorhombic to rhombohedral phase transition in $La_{2/3}(Ca_{1-x}Sr_x)_{1/3}MnO_3$ manganites, *J. Lumin.* 128, 5–6, 992-994, 2008, ISSN 0022-2313.

[170] A. Asamitsu, Y. Moritomo, Y. Tomioka, T. Arima, and Y. Tokura, A structural phase transition induced by an external magnetic field, *Nature (London)* 373, 407, 1995

[171] E. Brinza, Electrical and Magnetocaloric Properties of the $La_{0.7}Ba_{0.3-x}Ca_xMnO_3$ Compounds. Diploma Thesis, Babes-Bolyai University, Cluj-Napoca, Romania, 2022, *unpublished*.

[172] R. Atanasov, E. Brinza, R. Bortnic, R. Hirian, G. Souca, L. Barbu-Tudoran and I. G. Deac, Magnetic and Magnetocaloric Properties of Nano- and Polycrystalline Bulk Manganites $La_{0.7}Ba_{(0.3-x)}Ca_xMnO_3$ ($x \leq 0.25$), *Magnetochemistry 9*(7), 170, 2023.

[173] A. Szytula, Manganites — Structural Aspects, *Acta Physica Polonica Series a* 118(2), 2010.
[174] A. Gupta, at al, Grain boundary effects on the magnetoresistance properties of perovskite manganite films, *Phys. Rev. B* 54, R15629(R), 1996.
[175] A. Urishibara, at al, Insulator-metal transition and giant magnetoresistance in $La_{1-x}Sr_xMnO_3$, *Phys. Rev. B* 51, 14103, 1995.
[176] H. Qin, J. Hu, J. Chen, Y. Wang, Z. Wang, Giant magnetoimpedance and colossal magnetoresistance in $La_{0.75}Sr_{0.25}MnO_3$ at room temperature, *J. Appl. Phys.* 91, 10003, 2003.
[177] C.L. Lu, S. Dong, K.F. Wang, F. Gao, P.L Li, L.Y. Lv, J.M. Liu, Charge-order breaking and ferromagnetism in $La_{0.4}Ca_{0.6}MnO_3$ nanoparticles. *Appl. Phys. Lett*. 2007, *91*, 032502. 2007.
[178] N. S. Bingham; M. H. Phan; H. Srikanth; M. A. Torija; C. Leighton, Magnetocaloric effect and refrigerant capacity in charge-ordered manganites, *J. Appl. Phys.* 106, 023909, 2009.
[179] Q. Zhang, F. Guillou, A.Wahl, Y. Breard, and V. Hardy, Coexistence of inverse and normal magnetocaloric effect in A-site ordered $NdBaMn_2O_6$, *Appl. Phys. Lett.* 96, 242506, 2010.
[180] X.H. Zhang, Z.Q. Li, W. Song, X.W. Du, P.Wu, H.L. Bai, H.Y. Jiang, Magnetic properties and charge ordering in $Pr_{0.75}Na_{0.25}MnO_3$ manganite. *Solid State Commun*. *135*, 356, 2005.
[181] I.G. Deac, J. Mitchell, P. Schiffer, Phase Separation and the Low-Field Bulk Magnetic Properties of $Pr_{0.7}Ca_{0.3}MnO_3$. *Phys. Rev. B 63*, 172408, 2001.
[182] S.S. Rao, S. Tripathi, D. Pandey, S.V. Bhat, Suppression of charge order, disappearance of antiferromagnetism, and emergence of ferromagnetism in $Nd_{0.5}Ca_{0.5}MnO_3$ nanoparticles. *Phys. Rev. B, 74*, 144416, 2006.
[183] D. Ailenei, Electrical, magnetic and magnetocaloric properties in $Pr_{0.65}Sr_{0.35-x}Ca_xMnO_3$ compounds, Diploma Thesis, Babes-Bolyai University, Cluj-Napoca, Romania, 2022, *unpublished*.
[184] R. Atanasov, D. Ailenei, R. Bortnic, R. Hirian, G. Souca, A. Szatmari, L. Barbu-Tudoran and I. G. Deac, Magnetic Properties and Magnetocaloric Effect of Polycrystalline and Nano-Manganites $Pr_{0.65}Sr_{(0.35-x)}Ca_xMnO_3$ ($x \leq 0.3$), *Nanomaterials*, *13*(8), 1373, 2023.
[185] G. Cao; J. Zhang, S. Wang, J. Yu, C. Jing, S. Cao, X. Shen, Reentrant spin glass behavior in CE-type AFM $Pr_{0.5}Ca_{0.5}MnO_3$ manganite. *J. Magn. Magn. Mater*. *310*, 169, 2007.
[186] K.N. Anuradha; S.S. Rao; S.V. Bhat; Complete 'melting' of charge order in hydrothermally grown $Pr_{0.57}Ca_{0.41}Ba_{0.02}MnO_3$ nanowires. *Journal of Nanoscience and Nanotechnology*, 7, 1775–1778, 2007, doi: 10.1166/jnn.2007.713.
[187] D. Hüser; L.E. Wenger; A.J. van Duynevelt; J.A. Mydosh, Dynamical behavior of the susceptibility around the freezing temperature in (Eu,Sr)S. *Phys. Rev. B, 27*, 3100, 1983.
[188] R. Singh, S. K. Srivastava, A. K. Nigam, V. V. Khovaylo, L. K. Varga, R. Chatterjee, Use of Arrott plots to identify Néel temperature (T_N) in metamagnetic $Ni_{48}Co_6Mn_{26}Al_{20}$ polycrystalline ribbons, *J. Appl. Phys*. 114, 243911, 2013.
[189] P. Jain, at al, Investigation of Arrott plot and magnetocaloric effect in the complex $CaMn_7O_{12}$ perovskite, *cond-mat. mtrl-sci*, arXiv:1512.00618, 2015.
[190] N.S. Bingham, M.H. Phan, H. Srikanth, M.A. Torija, C. Leighton, Magnetocaloric effectand refrigerant capacity in charge-ordered manganites, *J. Appl. Phys*. 106, 023909, 2009.

[191] R. Atanasov, R. Hirian, R. Bortnic, G. Souca, A. Szatmari, Lucian Barbu-Tudoran and I. G. Deac, Near-room-temperature magnetic properties and magnetocaloric effect of Polycrystalline and Nano-scale manganites $Pr_{0.65-x}Nd_xSr_{0.35}MnO_3$ ($x \leq 0.35$), *J. Alloys compd.*, 1004, 175932, 2024.
[192] V. Franco, J.S. Blázquez, B. Ingale, A. Conde, The Magnetocaloric Effect and Magnetic Refrigeration Near Room Temperature: Materials and Models, *Annu. Rev. Mater. Res*. 42:305–42, 2012**,** https://doi.org/10.1146/annurev-matsci-062910-100356.
[193] R. M'nassri, N. Chniba-Boudjada, A. Cheikhrouhou, 3D-Ising ferromagnetic characteristics and magnetocaloric study in $Pr_{0.4}Eu_{0.2}Sr_{0.4}MnO_3$ manganite, *J. Alloys Compd.*, 640, pp.183-192, 2015, ISSN 0925-8388, https://doi.org/10.1016/j.jallcom.2015.03.220.
[194] A. Kumar, at al, Large magnetocaloric effects in Pr-doped $La_{1.4-x}Pr_xCa_{1.6}Mn_2O_7$ bilayer manganites, *J. Alloys Compd*. 845, 2020.
[195] N. Qin, at al, Structural and Thermoelectric Properties of $Gd_{2-2x}Sr_{1+2x}Mn_2O_7$ Double-Layered Manganites, *Materials*, *16*(7), 2548, 2023.
[196] T. Kimura, Y Tokura, Layered magnetic manganites, *Annu. rev. mater. sci*., 30, 451-474, 2000.
[197] B. Zhao *et al.*, The Magnetic Properties and Magnetocaloric Effect of $Pr_{0.7}Sr_{0.3}MnO_3$ Thin Film Grown on SrTiO3 Substrate. *Materials (Basel)*, 16, 1, 2023, doi: 10.3390/ma16010075.
[198] S. Canulescu, at al, *Magnetic properties of solids*, Nova science publishers, 179-202, 2009.